Peierls and Spin-Peierls Instabilities in the Per2[M(mnt)2] Series of One-Dimensional Organic Conductors; Experimental Realization of a 1D Kondo Lattice for M = Pd, Ni and Pt

Jean-Paul Pouget, Pascale Foury-Leylekian, Manuel Almeida

Peierls and Spin-Peierls Instabilities in the $Per_2[M(mnt)_2]$ Series of One-Dimensional Organic Conductors; Experimental Realization of a 1D Kondo Lattice for M = Pd, Ni and Pt

Jean-Paul Pouget 1, Pascale Foury-Leylekian 1 and Manuel Almeida 2

1 Laboratoire de Physique des Solides, Université Paris-sud, CNRS UMR 8502, F91405 Orsay, France

2 C2TN—Centro de Ciências e Tecnologias Nucleares, Instituto Superior

magnetochemistry

MDPI

Review

Peierls and Spin-Peierls Instabilities in the $Per_2[M(mnt)_2]$ Series of One-Dimensional Organic Conductors; Experimental Realization of a 1D Kondo Lattice for M = Pd, Ni and Pt

Jean-Paul Pouget [1,*], Pascale Foury-Leylekian [1] and Manuel Almeida [2]

[1] Laboratoire de Physique des Solides, Université Paris-sud, CNRS UMR 8502, F91405 Orsay, France; pascale.foury@u-psud.fr

[2] C2TN—Centro de Ciências e Tecnologias Nucleares, Instituto Superior Técnico, Universidade de Lisboa, P-2695-066 Bobadela LRS, Portugal; malmeida@ctn.tecnico.ulisboa.pt

* Correspondence: jean-paul.pouget@u-psud.fr

Academic Editor: Carlos J. Gómez García

Received: 25 January 2017; Accepted: 17 February 2017; Published: 25 February 2017

Abstract: We consider structural instabilities exhibited by the one-dimensional (1D) $(arene)_2X$ family of organic conductors in relation with their electronic and magnetic properties. With a charge transfer of one electron to each anion X, these salts exhibit a quarter-filled (hole) conduction band located on donor stacks. Compounds built with donors such as fluorenthene, perylene derivatives and anions X such as PF_6 or AsF_6 exhibit a high temperature (T_P ~170 K) conventional Peierls transition that is preceded by a sizeable regime of 1D $2k_F$ charge density wave fluctuations (k_F is the Fermi wave vector of the 1D electron gas located on Per stack). Surprisingly, and probably because of the presence of a multi-sheet warped Fermi surface, the critical temperature of the Peierls transition is considerably reduced in the perylene series α-$(Per)_2[M(mnt)_2]$ where X is the dithiolate molecule with M = Au, Cu, Co and Fe. Special attention will be devoted to physical properties of α-$(Per)_2[M(mnt)_2]$ salts with M = Pt, Pd and Ni which incorporate segregated S = 1/2 1D antiferromagnetic (AF) dithiolate stacks coexisting with 1D metallic Per stacks. We analyze conjointly the structural and magnetic properties of these salts in relation with the 1D spin-Peierls (SP) instability located on the dithiolate stacks. We show that the SP instability of Pd and Ni derivatives occurs in the classical (adiabatic) limit while the SP instability of the Pt derivative occurs in the quantum (anti-adiabatic) limit. Furthermore, we show that in Pd and Ni derivatives 1st neighbor direct and frustrated 2nd neighbor indirect (through a fine tuning with the mediated $2k_F$ RKKY coupling interaction on Per stacks) AF interactions add their contribution to the SP instability to stabilize a singlet-triplet gap. Our analysis of the data show unambiguously that magnetic α-$(Per)_2[M(mnt)_2]$ salts exhibit the physics expected for a two chain Kondo lattice.

Keywords: One dimensional organic conductor; Peierls transition; spin-Peierls transition; Kondo lattice; frustrated antiferromagnetic chain

1. Introduction

Since the discovery of the so-called Peierls transition in the Krogmann salt $K_2Pt(CN)_4Br_{0.3}$-$3H_2O$ (KCP) [1] in 1973, nearly than 45 years ago, many investigations have shown that most one-dimensional (1D) conductors are subject to a coupled electronic-structural instability transition at the $2k_F$ critical wave vector (k_F being the Fermi wave vector of the 1D electron gas). Due to the electron–phonon coupling the Peierls transition consists in a $2k_F$ modulated wave of bond distances, forming a so-called bond ordered wave (BOW), accompanied by a $2k_F$ modulation of the electronic density, forming

a so-called charge density wave (CDW); these two waves being in quadrature (see [2]). The $2k_F$ modulation wave vector related to the 1D band filling is generally in incommensurate relation with the chain reciprocal wave vector, noted b* below ($2k_F$, expressed in b* reciprocal unit, amounts to half the number of conduction electrons, ρ, per repeat unit; the factor 2 is due to the spin degree of freedom). At the Peierls transition, T_P, the long range $2k_F$ modulation, which opens a gap at the Fermi level in the 1D band structure, drives a metal to insulator phase transition. However, because of the 1D nature of the underlying electronic instability, the Peierls transition is preceded by a very sizable regime of 1D $2k_F$ CDW/BOW fluctuations which extends up to 2–4 times T_P (the onset temperature of CDW/BOW fluctuations corresponds to about the mean-field Peierls temperature, T_P^{MF} defined more precisely below). Between T_P^{MF} and T_P, local fluctuations in direct space open a partial gap (i.e., a pseudo-gap) in the electronic structure. More explanations concerning these distinctive features can be found in a recent review [3].

$2k_F$ Peierls transitions are well observed in quasi-1D inorganic compounds such as the Krogmann salts, the blue bronzes, $K_{0.3}MoO_3$, and the transition metal tri-chalcogenides, $NbSe_3$ and TaS_3, built with chain of transition elements based inorganic polyhedron ($Pt(CN)_4$ square, MoO_6 octahedron and $NbSe_6/TaS_6$ anti-prism, respectively) between which there is a strong overlap of d wave functions [4]. Other significant examples can be found among organic conductors built with stacks of planar molecules between which there is a sizeable overlap of p_π molecular orbitals (MO). In organic salts, the metallic character is achieved either by a partial charge transfer ρ from stacks of donor (D) to stacks of acceptor (A), such as in TTF-TCNQ, or by a complete charge transfer from anion (X)/cation (Y) to D/A in 2:1 D_2X or A_2Y salts (TTF = tetrathia-fulvalene, TCNQ = tetracyano-quinodimethane). Only D_2X salts, with ρ = 1/2 hole charge transfer, will be considered in this paper (in these salts, the band structure built on the donor HOMO is quarter-filled in hole). An important characteristic of organic metals is that, with a stack built with tilted large planar molecules, the HOMO nodal structure leads to intra-stack transfer integral ($t_{//}$) often smaller or comparable to intra-molecular (U) or inter-molecular (V) Coulomb repulsion terms. Thus because of the relative importance of electron repulsions U and V with respect to $t_{//}$, organic conductors develop also another type of CDW instability at the critical $4k_F$ wave vector consisting in a Wigner (or Mott-Hubbard) type of charge localization [2]. Thus, as a non-degenerate HOMO level can be at most occupied by an hole whatever its spin, the critical wave vector of the charge localization mechanism, being associated to ρ, is $4k_F$ in 1D. In 2:1 organic salts, intensively studied in recent years [5], a spin-charge decoupling accompanies the charge localization phenomenon. When such a decoupling is achieved, the localized S = 1/2 degrees of freedom remain available to order in anti-ferromagnetic (AF) or non-magnetic singlet paired ground states. The singlet pairing is generally stabilized by a dimerization of the chain of localized spins. The transition which thus results opens a singlet-triplet gap in the AF magnetic excitation spectrum. Being analog to the metal-insulator Peierls transition, which opens a gap in a metallic excitation spectrum, the singlet pairing transition is called for this reason a spin-Peierls (SP) transition whose main characteristics are now well documented in the recent literature (see for example Reference [3,5]).

The perylene (Per) molecule, shown in Figure 1a, has played an important role in the development of the field of 1D organic conductors because the first molecular crystal exhibiting a metallic conductivity was found in 1954 when Per was exposed to Br [6]. Then many family of organic salts based on the Per donor and its derivatives were found to exhibit metallic properties [7]. Among them, 2:1 D_2X salts were found to be quasi-1D metals exhibiting a $2k_F$ BOW/CDW instability diverging into a Peierls metal-insulator transition (see Section 2). A very original physics is observed in the α phase of Per-dithiolate salts, named α-$(Per)_2[M(mnt)_2]$ below, which mix 1D conducting and magnetic properties [7,8] (another β phase is semiconducting [7]). The structure of α-$(Per)_2[M(mnt)_2]$ exhibits along the b direction (perpendicular to the plane of Figure 2) regular stacks of tilted and partially oxidized Per molecules which coexist with metal-bisdithiolene complex $[M(mnt)_2]^-$ stacks. $[M(mnt)_2]^-$, shown in Figure 1b, is a close shell molecule for M = Au and Cu, while $[M(mnt)_2]^-$ bears an unpaired spin 1/2 for M = Ni, Pd and Pt. Due to the charge transfer of one electron per dithiolate,

leaving ρ = 1/2 hole per Per, α-$(Per)_2[M(mnt)_2]$ forms a family of high conducting and anisotropic conductors (σ_b ~700 S/cm and $\sigma_b/\sigma_\perp$ ~10^3 at RT) [9] with a quarter-filled hole (or a three quarter filled electron) conduction band—see Figure 3a. With regular stacks of *M* = Au and Cu close shell dithiolate molecules and dimerized stacks of *M* = Fe and Co dithiolate molecules, only the Per stack is electro-active. These systems exhibit a Peierls instability that was reported more than 25 years ago [8]. Its salient features will be summarized in Section 2 and compared to those shown by other D_2X salts of arene donors. Magnetic α-$(Per)_2[M(mnt)_2]$ salts incorporating dithiolate stacks with *M* = Ni, Pd and Pt are very original systems since dithiolate stacks, where each $[M(mnt)_2]^-$ bears a spin S = 1/2, coexist with conducting Per stacks subject to a Peierls instability. In addition, these regular dithiolate stacks forming S = 1/2 AF chains are subject to a SP instability [9]. The SP instability of the dithiolate stacks was however poorly studied. Thus, a complete analysis of their SP instability will be object of Section 3. Section 3 will also consider the unprecedented coupling between the SP and Peierls instabilities from which a new physics emerges.

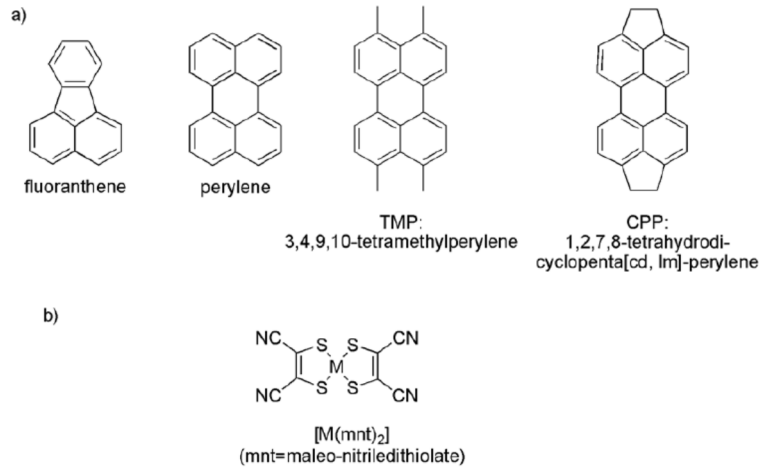

Figure 1. Chemical structure of: (**a**) fluoranthene (FA), perylene donors and its derivatives TMP and CPP; and (**b**) the dithiolate acceptor $[M(mnt)_2]$.

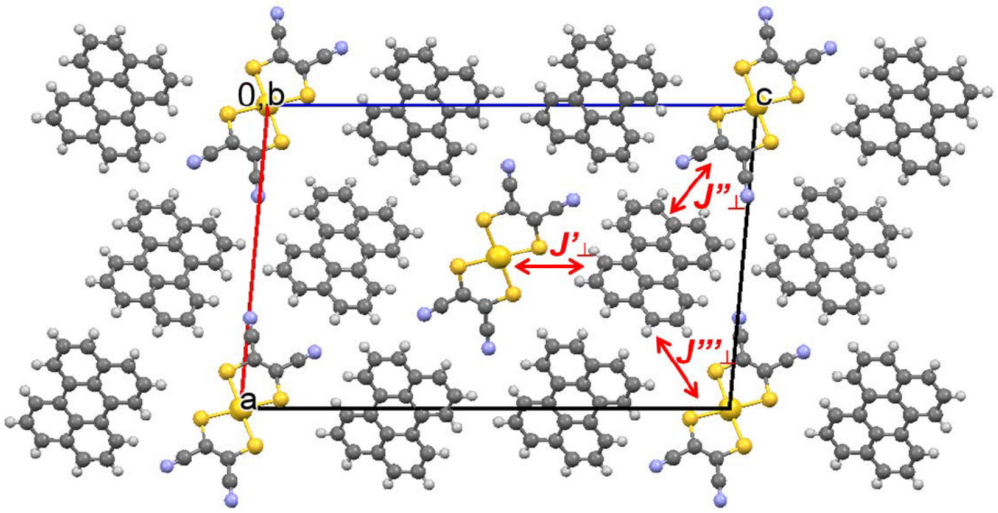

Figure 2. Crystal structure of α-$Per_2[M(mnt)_2]$ projected along the stack direction b, which shows the presence of segregated Per and dithiolate stacks. In this structure, each $[M(mnt)_2]$ stack fills tunnel delimited by six Per stacks, and there is one Per stack inside each triangular array of first neighbors $[M(mnt)_2]$ stacks. First neighbor inter-stack $[M(mnt)_2]$—Per AF exchange coupling $J_\perp$ are schematically indicated (note that there are three different types of interactions per Per).

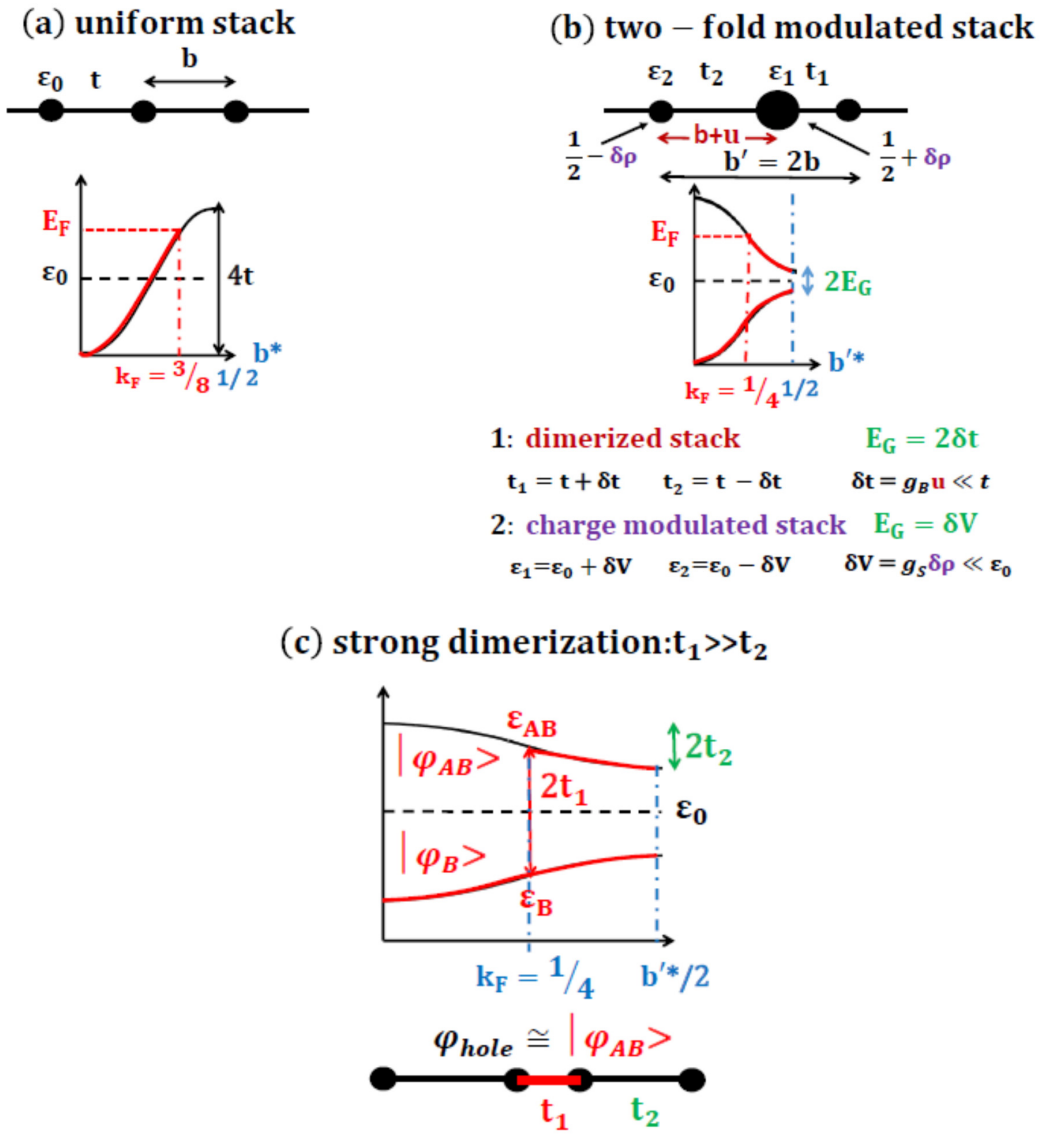

Figure 3. Three-quarter electron (one-quarter hole) filled band structure of D_2X arene salts for: a uniform donor stack (**a**); and a two-fold modulated donor stack (**b**). The positive band dispersion is due to the graphitic type of overlap of donor molecules. (**b**) considers the two extreme situations : (1) of a dimerized stack, and (2) of a charge modulated stack. The expression of the band gap $2E_G$ at the Brillouin zone boundary b'*/2 is given in (1), for a small modulation of transfer integrals t, and in (2) for a small modulation of site energies ε. The case of a strongly dimerized stack is considered in (**c**). In this situation the wave functions/energies are basically that of well decoupled bonding /Ψ_B>/ε_B and anti-bonding /Ψ_{AB}>/ε_{AB} states of the dimer. For a one quarter hole band filling, the system can be considered as having an half-filled AB band where the hole wave function is basically localized in the anti-bonding state of the dimer.

2. Peierls Instability in Per_2X Salts and Its Per Substituted Derivatives

In this section, we summarize the Peierls instabilities exhibited by various D_2X arene cation radical salts whose main characteristics are given in Table 1. This table shows that depending of the salt the donor stack can be either uniform or two-fold modulated. In the second case, two-fold bond or site modulations of the donor stack periodicity are generally the consequence of specific interactions with intrinsically dimerized anion stacks or with chemically alternated anion-solvent columns. Such differentiated interactions will either modulate inter-donor bond distances and/or

modulate the external potential on donor sites with the consequence to modulate electronic parameters such as the intra-stack transfer integral t or the one-electron site energy ε (see Figure 3b). In all these cases, there is a band folding in b*/4 or b'*/2 together with the opening of a band gap $2E_G$, whose expression is given in Figure 3b. Furthermore, if there is a lateral disorder between columns of anions surrounding a given donor stack, the modulation of the stack will be also disordered.

1D CDW systems are very sensitive to disorder. Disorder either limits the lifetime of electron–hole pairs of wave vector $2k_F$, which are the building blocks of the CDW, or pins the phase of the $2k_F$ BOW/CDW modulation. Electron backscattering on impurities reverses the wave vector of one constituent of the electron–hole pair (let say from $+k_F$ to $-k_F$), which destroy the CDW pairing. Consequently, the backscattering process gives a finite lifetime at the electron–hole pair. This lifetime effect depresses the Peierls transition, as observed in the solid solution $Per_2[Au_xPt_{1-x}(mnt)_2]$ [10]. Local pinning of the phase of the CDW on a random distribution of lattice defects limits the longitudinal and transverse spatial coherence of the 3D CDW order (for more details see [3]).

Table 1. Characteristics of arene cation radical salts exhibiting a Peierls instability. The table gives the structure of the donor stack. The Peierls transition temperature (T_P) and the temperature of minimum of resistivity (T_ρ) are taken from conductivity measurements of Ref. [7,8]. The mean field Peierls temperature (T_P^{MF}) is calculated from the electrical gap $2\Delta_0$ using Equation (2). The dimension and temperature range of $2k_F^D$ BOW pre-transitional fluctuations are also indicated. [a] Dithiolate sacks composed of strongly paired $[Fe(mnt)_2]$ or $[Co(mnt)_2]$ units should induce a doubling of the Per stack periodicity. The expected Per two-fold stack deformation due to its dimerized surrounding has not been determined in the Co compound [11], but it has been recently found to be small in the Fe compound [12]. [b] The question mark leaves open a possible doubling of CPP stack periodicity induced by its surrounding of alternated anion–solvent columns [13]. [c] A doubling of TMP stack periodicity is expected from the detection of a charge order (i.e., $4k_F$ CDW) on donor stack by ^{13}C-CPAS-NMR [13]. However, local NMR measurement is unable to probe the spatial extend of this order.

Compound	Donor Stacking	T_P (K)	$2k_F^D$ BOW Pre-Transitional Fluctuations	T_ρ (K)	T_P^{MF} (K)
$Per_2[Cu(mnt)_2]$	Uniform	32	not observed	40	66
$Per_2[Au(mnt)_2]$	Uniform	12	not observed	16	11.5
$Per_2[Fe(mnt)_2]$	Dimerized [a]	73	3D ≤ 80 K	180	165
$Per_2[Co(mnt)_2]$	Dimerized [a]	58	3D ≤ 65 K	160	200
$(CPP)_2PF_6 + CH_2Cl_2$	Uniform? [b]	158	1D above RT	>300	?
$(CPP)_2AsF_6 + CH_2Cl_2$	Uniform? [b]	170	1D above RT	?	?
$(TMP)_2PF_6 + CH_2Cl_2$	$4k_F$ site CDW [c]	<20	1D ≤ 210 K	>300	?
$(TMP)_2AsF_6 + CH_2Cl_2$	$4k_F$ site CDW [c]	<20	1D ≤ 200 K	?	?
$(FA)_2 PF_6$	Dimerized	180	1D above RT	>300	400–600

2.1. Uniform Stack

For ρ = 1/2 hole per arene, the 1D donor band structure is quarter-filled in holes ($\frac{3}{4}$ filled in electrons)—see Figure 3a. For an uniform stack of periodicity b, the critical Peierls wave vector is $2k_F^D$ = b*/4 for the hole filling ($2k_F^D$ = 3b*/4 for the electron filling). In the mean field approximation (which neglects 1D pre-transitional $2k_F^D$ fluctuations), the Peierls transition occurs for:

$$T_P^{MF} \approx C\, E_F e^{-1/\lambda_{2k_F}} \quad (1)$$

In Equation (1), E_F is the hole Fermi energy and, since $2k_F$ phonons pair a $-k_F$ hole to a $+k_F$ electron, λ_{2k_F} is the reduced $2k_F$ electron–phonon coupling [3]. C is a constant, of few units, which depends on the shape of the band dispersion near E_F (for a free electron dispersion C ≈ 2.25). The Peierls transition opens a gap 2Δ at $\pm k_F$ in the 1D band structure. At 0 K, the gap $2\Delta_0$ is related to $T_P{}^{MF}$ by the BCS-type correspondence law:

$$2\Delta_0 = 3.56 T_P^{MF} \quad (2)$$

Table 1 reports $T_P{}^{MF}$ deduced, via Equation (2), from the activation energy Δ_0 of the conductivity measured below T_P.

Note that with $2k_F^D$ = b*/4, the Peierls superstructure stabilizes a 4b periodicity in stack direction. Since 4 × $2k_F^D$ = b*, the $2k_F$ BOW/CDW modulation wave length is in fourth-fold commensurate relation with the chain periodicity b, so that the phase of the CDW modulation should be pinned in the structure by the four-fold lattice potential.

2.2. Two-Fold Modulated Stack

Table 1 shows that in many salts the donor stack periodicity is doubled. In that case with a stack periodicity b' = 2b, the critical Peierls wave vector should be $2k_F^D$ = b'*/2 (see the folded band structure shown in Figure 3b). Note also that the new reciprocal periodicity b'* of the two-fold modulated structure amounts to $4k_F^D$ which is the critical wave vector associated to a charge localization phenomena (see Section 1). In such a modulated structure, the band folding opens a band gap $2E_G$ at ±b'*/2 due either to a dimerization of the stacks or to the presence of non-equivalent donor sites. Generally the bond dimerization due to successive molecular shifts $\pm u/2$ (leading to a differentiation of transfer integral by $\delta t = g_B u$) or to a charge unbalance on each donor $\pm\delta\rho$ (leading to a difference of HOMO potential energy $\delta V = g_S \delta\rho$) are small quantities, so that with $E_G = 2\delta t$ or $E_G = \delta V$ one has $E_G << t$ (in these last expressions g_i is the bond (B) or site (S) electron–phonon coupling and t is the transfer integral of the uniform stack). Note that in these situations the underlying dimerization or charge modulation effect can be viewed as achieved by the presence of a static $4k_F$ BOW or $4k_F$ CDW, of amplitude $u/2$ or δρ, respectively, on the Per stack. For a weak modulation and for a weakly interacting electron gas, these effects do not change appreciably the physics of the Peierls instability with respect to the one of a quarter-filled band. In particular, the $2k_F$ BOW/CDW modulation remains mainly pinned on the structure by a fourth-order lattice potential as for the uniform stack (the two-fold pinning lattice potential proportional to u or δρ being much smaller). This statement is not true for a sizeable band gap $2E_G$ in presence of strong electron repulsions where the $4k_F$ electron-electron scattering Umklapp term induces a $4k_F$ BOW or $4k_F$ CDW charge localization as observed for example in Fabre salts $(TMTTF)_2X$ [14]; TMTTF = tetramethyl-tetratia-fulvalene.

In the case of a strong dimerization shown in Figure 3c, where $t_{intra} >> t_{inter}$, bonding and anti-bonding states of the dimer are well decoupled in energy. Thus one hole tends to be localized on the anti-bonding state of each dimer, and the anti-bonding band can be considered as half-filled. In this situation equivalent to an half-filled 1D system, each dimer can be considered as a rigid unit and the $2k_F$ BOW/CDW of wave length 2b' will basically modulate the inter-dimers distances. There is thus strong pinning of the $2k_F$ CDW on each dimer by a two-fold lattice potential.

In the case of a two-fold modulated stack, there is an additional process entering in the $2k_F$ electron–phonon coupling Peierls mechanism. Since one has $4k_F^D$ = b'*, umklapp scattering processes should also contribute to the $2k_F$ electron–phonon coupling mechanism. The associated reduced electron–phonon coupling constant, λ_{um}, which is proportional to the amplitude of the $4k_F$ BOW or of the $4k_F$ CDW, adds to λ_{2k_F} in Equation (1). One simply gets, in the mean-field approximation, the relation:

$$T_P^{MF} \approx C\, E_F e^{-1/(\lambda_{2k_F} + \lambda_{um})} \quad (3)$$

In the limit of a strongly dimerized stack the contribution of umklapp processes could be of the same magnitude as the normal $2k_F$ electron–phonon coupling process. In that case with $2\lambda_{2k_F} \approx \lambda_{2k_F} + \lambda_{um}$, one obtains an enhanced mean-field Peierls transition temperature given by:

$$T_P^{MF} \approx C E_F e^{-1/2\lambda_{2k_F}} \quad (4)$$

2.3. Estimation of the Electron-Phonon Coupling

In a 3D solid made by a collection of weakly coupled chains, the true 3D Peierls transition temperature, $T_{P,}$ is generally depressed by a sizeable fraction of $T_P{}^{MF}$ (see Table 1). This is due the presence of an important regime of 1D structural fluctuations which destroy the mean-field 1D order between ~T_P^{MF} and T_P [3]. In that temperature range, local 1D $2k_F$ lattice fluctuations form a pseudo-gap in the electronic density of states, which corresponds to a local formation of the Peierls gap. As the pseudo-gap reduces progressively the effective number of carriers in the vicinity of the Fermi level it is generally accompanied by an upturn at T_ρ in the thermal dependence of the electrical conductivity (T_ρ ~$T_P^{MF} > T_P$, see Table 1) and by its decreases below T_ρ. Note that in a pure 1D system 1D CDW and BOW thermal fluctuations completely suppress the Peierls transition. The non-zero value of T_P reported in Table 1 is due to inter-chain coupling (several relevant mechanisms are described in Ref. [3]).

Using Equation (1) or (4) for uniform or strongly two fold modulated stacks, it is possible to estimate λ from the knowledge of $T_P{}^{MF}$ and E_F. In α-(Per)$_2$[M(mnt)$_2$] the linear thermal dependence of the hole-like thermo-power leads to a bandwidth of $4t_{//}$ = 0.6eV [7,8] which gives for a quarter filled 1D hole band $E_F = \sqrt{2}t_{//}$≈0.2eV. Using a free hole dispersion in the vicinity of E_F, as assessed by the band structure calculation of Ref. [15], one gets with $T_P{}^{MF} \approx T_\rho$ in Equation (1):

$$\lambda_{2k_F} \sim 0.2 \text{ for the M} = \text{Au salt} \quad (5)$$

$$\lambda_{2k_F} \sim 0.25 \text{ for the M} = \text{Cu salt} \quad (6)$$

Assuming a sizable Per stack dimerization due to the chemical bonding of M(mnt)$_2$ units into dimers, one gets using Equation (4):

$$\lambda_{2k_F} \sim 0.2 \text{ for the M} = \text{Fe and Co salts} \quad (7)$$

These values are comparable to λ_{2k_F} calculated with Equation (1) in KCP (0.2) and in the blue bronze $K_{0.3}MoO_3$ (0.25).

If one assumes the same band width in (FA)$_2$ PF_6 as in α-(Per)$_2$[*M*(mnt)$_2$] one gets, with Equation (1) which neglects the stack dimerization (see below), λ_{2k_F} = 0.6. A similar reduced sizable electron-coupling λ_{2k_F} = 0.6 is obtained for the trans-polyacetylene, $(CH)_x$.

2.4. Peierls Instability in (Arene)$_2$ PF$_6$ and AsF$_6$ Salts

Table 1 shows that D_2X salts where D is fluoranthene (FA) or perylene derivatives substituted with four methyl groups (TMP) or two cyclopentanes (CPP) (Figure 1a) exhibit, in presence of monovalent anions such as *X* = PF_6 and AsF_6, a sizable regime of 1D $2k_F$ fluctuations pre-transitional to the Peierls transition. Such 1D $2k_F$ BOW fluctuation regime, associated to a significant electron–phonon coupling, have been detected in the FA, CPP and TMP salts by X-ray diffuse scattering measurements [13,16–18]. In (CPP)$_2AsF_6$ + CH_2Cl_2 the susceptibility associated to the 1D $2k_F$ BOW instability, $\chi_{BOW}(2k_F)$, follows a Curie–Weiss dependence (which corresponds to a regime of Gaussian fluctuations of the amplitude of the order parameter) which diverges at a 2nd order Peierls transition at T_P = 170 K (Figure 4) [18]. Similar results are obtained in (FA)$_2PF_6$ [16]. $2k_F$ BOW/CDW fluctuations strongly affect the electron density of states at the Fermi level by forming a pseudo-gap, precursor to the Peierls gap. This progressively reduces the effective number of carriers available for the charge transport so that the electrical conductivity measured in these systems decreases in the temperature range of existence of 1D fluctuations below T_ρ ~T_P^{MF} [17–20]. All these features are those of a conventional Peierls instability.

In most of the salts, $2k_F$ fluctuations are 3D coupled at the Peierls transition at T_P which thus stabilizes a 3D long range order (LRO) of $2k_F$ BOW/CDW modulations. This 3D Peierls transition is characterized by the appearance below T_P of $2k_F$ superstructure reflections whose intensity $I_{sat}(\boldsymbol{q_P})$

is proportional to the square of the amplitude of the BOW/CDW modulation (see Figure 4 for $(CPP)_2AsF_6 + CH_2Cl_2$ [13,18]).

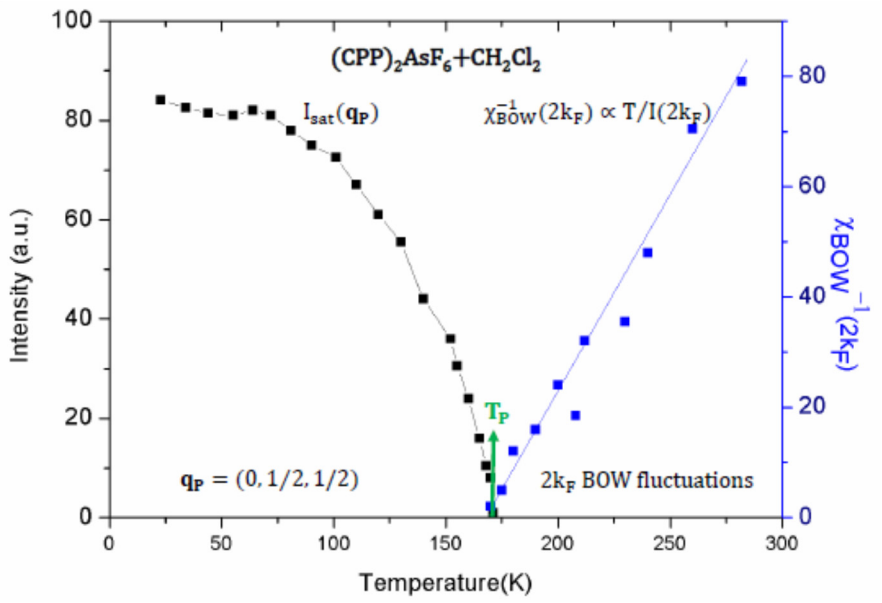

Figure 4. Temperature (T) dependence of the inverse of the $2k_F$ BOW susceptibility $\chi^{-1}_{BOW}(2k_F)$ above T_P and of the $2k_F$ Peierls satellite intensity $I_{sat}(\boldsymbol{q_P})$ below T_P in $(CPP)_2AsF_6 + CH_2Cl_2$ (adapted from [13,18]). $\chi^{-1}_{BOW}(2k_F)$ is proportional to $T/I(2k_F)$, where $I(2k_F)$ is the intensity of the X-ray diffuse lines at $2k_F$.

In the Peierls ground state of $(FA)_2PF_6$ it has been observed that the $2k_F$ BOW/CDW modulation could collective slide under the action of an external electric field exceeding a threshold field value of E_T ~0.2 V/cm [19,20]. As the threshold field depends on the pinning energy of the CDW on impurity and on the order of commensurability of the lattice potential, the finding of a similar E_T in dimerized $(FA)_2PF_6$ and in α-$(Per)_2Au(mnt)_2$ (E_T ~0.5 V/cm [21]) exhibiting a regular Per stack means that the pinning is mainly achieved by the fourth-order lattice potential in $(FA)_2PF_6$. Thus, the $2k_F$ CDW modulation is basically that of a quarter filled band in $(FA)_2PF_6$.

Table 1 shows that TMP and CPP salts incorporate one solvent molecule (S = CH_2Cl_2) per anion, X. This leads to the formation of mixed X-S columns in stack direction with a short range lateral order between neighboring X-S columns [13]. In CPP, inter-columnar disorder does not prevent the occurrence of a high temperature Peierls transition at T_P = 158–170 K (see Table 1 and Figure 4). $(TMP)_2AsF_6 + CH_2Cl_2$ exhibits also a sizeable regime of $2k_F$ fluctuations below ~200 K, but at the difference of its CPP analog it exhibits only a short range lateral BOW order at 20 K [18]. The absence of a 3D long range BOW order could be due a strong pinning of the $2k_F$ modulation on X-S disorder. In addition, and by analogy with earlier findings in the $[(TMTSF)_{1-x}(TMTTF)_x]_2ReO_4$ solid solution [22], the divergence of the $2k_F$ BOW instability could be inhibited by the existence of a $4k_F$ CDW order on the TMP stack already at RT.

2.5. Peierls Instability in Per Stack of α-$(Per)_2[M(mnt)_2]$

α-$(Per)_2[M(mnt)_2]$ salts with M = Au, Cu, Fe and Co exhibit a quite small Peierls modulation which is assessed by the detection below T_P of extremely weak superlattice reflections at the $2k_F^D = 1/4b^*$ reciprocal position in the Cu salt [23] and somewhat stronger reflections at the $2k_F^D = 1/2b'^*$ reciprocal position in dimerized Fe and Co salts [24]. No superlattice reflections have been detected up to now in the Au salt (however one expects from the relative magnitude of Peierls gaps superlattice reflections one order of magnitude smaller in the Au salt than in the Cu salt). Probably because of the weakness

of the Peierls instability in all these salts the pre-transitional regime of 1D $2k_F$-BOW fluctuations could not be detected. Their characteristics temperature T_P, T_ρ and $T_P{}^{MF}$ are reported in Table 1.

The $2k_F^D$ = 1/4b* CDW stabilized below T_P in the Au compound collectively slides under the action of an external electric field exceeding E_T ~0.5 V/cm and exhibits the basic features of non-linear conductivity phenomena observed in CDW inorganic systems such as the blue bronze and the transition metal tri-chalcogenides [21,25]. Note, however, that the detection of a much larger threshold field E_T ~9 V/cm in the Pt salt [25] could be explained by the presence of a two-fold lattice pinning potential brought by the SP dimerization of the [Pt(mnt)$_2$] stacks (see below in Section 3).

As expected for a standard Peierls system, the critical temperature T_P of the Au compound decreases as H^2 for modest magnetic fields [26]. More interestingly, the CDW ground state is found to be unstable for large magnetic fields H_c ~33–37 T exceeding the so-called Pauli limit $H_P \approx 22.5$ T [27,28]. In addition, unexpected features observed near H_c suggest the occurrence of field induced CDW states due to orbital effects related to the presence of a warped Fermi surface (FS) [28,29].

Because of the presence of two slightly shifted sets of double quasi-1D warped FS [15] combined with the opening of a Peierls gap only slightly larger than inter-stack transfer integrals ($t_\perp$~2 meV), a destabilization of the Peierls instability of the Au compound is expected when pressure enhances the nesting breaking components of the FS. More precisely, it has been calculated [30] for a system exhibiting a warped FS incompletely nested by the $2k_F$ wave vector that the Peierls ground state should vanish when Δ_0 becomes smaller than the typical energy of hole and electron pockets remaining after the incomplete FS nesting process. Indeed it has been observed a vanishing of the CDW ground state of the Au compound above $P_c \approx 5$ kbar. More interestingly it is found, when the low temperature metallic state is restored under pressure, that α-(Per)$_2$[Au(mnt)$_2$] becomes a superconductor below T_S ~0.3 K [31].

Finally, it is interesting to remark that the weak Peierls gap, $2\Delta_0 \approx 3.5$ meV, of the Au salt [7,8] is smaller than a typical acoustic phonon frequency (Ω_c ~4.5–7 meV in TTF-TCNQ for $2k_F$ = 3/4b* [32]). Thus, with $2\Delta_0 < \hbar\Omega_c$, the Peierls transition of the Au salt should occur in the non-adiabatic regime [33]. The situation should be contrasted to that of the Cu salt where with $2\Delta_0 \approx 20$ meV $> \hbar\Omega_c$ [7,8] the Peierls transition should occur in the adiabatic regime, as for the (arene)$_2$ PF_6 and AsF_6 salts previously considered.

Note that in the non-adiabatic regime the 0 K amplitude of the Peierls gap should be reduced by quantum fluctuations from its mean-field value given by the BCS relation-ship (2). In addition, the non-adiabaticity of the Peierls mechanism should increase under pressure because of the hardening of the frequency of phonon modes. This effect should reduce the Peierls gap, and the vanishing of the CDW ground state in the Au salt under pressure should occur at a quantum critical point.

2.6. Comparison between Peierls Instabilities in (Arene)$_2PF_6$/AsF$_6$ and in α-(Per)$_2$[M(mnt)$_2$] Salts

While the donor stack of all these different families are made with molecules of similar chemical characteristics, there is a sizeable difference between Peierls instabilities in FA and CPP salts and those in Per salts. There is in particular a difference of more than a factor two in the Peierls transition temperature T_P and in the temperature range [T_ρ-T_P] of 1D CDW fluctuations for these two series of salts. As seen in Table 1, T_ρ occurs well above RT for FA and CPP salts while T_ρ is around 160–180 K (~2 times T_P) for the M = Co and Fe derivative and very close to T_P for the Cu and Au derivatives. Table 2 shows that, in the M = Ni, Pd and Pt derivatives, T_P and T_ρ are comparable to those of the Au and Cu derivatives.

A possible explanation relies on the number of donor conduction bands crossing the Fermi level (and also on the importance of their warping): one band for CPP and TMP salts, two bands for FA salt and four bands for Per salts. In the case of α-(Per)$_2$[M(mnt)$_2$], the total FS includes four sheets composed of two slightly shifted sets of warped open FS [15]. With such a band structure, the best nesting wave vector of the global FS should be poorly defined. The poor FS nesting should smoothen the thermal divergence of the $2k_F$ electron–hole response function [30] and thus reduces $T_P{}^{MF}$ and T_P.

A somewhat similar situation is found in the quarter-filled $(TSeT)_2Cl$ organic salt which, with a poorly nested FS composed of four warped sheets, exhibits a modest Peierls transition at T_P = 26 K [34] (TSeT = tetraseleno-tetracene).

3. Peierls and Spin-Peierls Instabilities in α-$(Per)_2M(mnt)_2$] with *M* = Ni, Pd and Pt

A special attention must be devoted to Per salts incorporating $[M(mnt)_2]$ acceptors with *M* = Ni, Pd and Pt, because the charge transfer from Per to dithiolate complexes leads to the formation of spin $\frac{1}{2}$ magnetic $[M(mnt)_2]^-$ species. One thus obtains two types of electro-active donor and acceptor stacks. However, at variance with TTF-TCNQ where the incommensurate charge transfer gives rise to two types of conducting stacks, each subject to its own CDW instability, the $[M(mnt)_2]^-$ stack is not conducting because there is a Mott–Hubbard localization of one electron per $[M(mnt)_2]$. With such a charge localization each $[M(mnt)_2]^-$ molecule bears an unpaired spin $\frac{1}{2}$. One thus obtains S = 1/2 AF coupled dithiolate stacks which coexist with metallic Per stacks in the same structure (Figure 2). As for the *M* = Au and Cu derivatives, Per stacks of the Pt, Pd and Ni derivatives are subject to a Peierls instability whose main characteristics are given in Table 2.

At the difference of the α-$Per_2[M(mnt)_2]$ series, it is interesting to remark that with an incommensurate charge transfer of 0.82 electron from Li to $[Pt(mnt)_2]$, the 1D conductor $Li_{0.82}[Pt(mnt)_2](H_20)_2$, whose stack structure resembles to some extend to that of KCP, undergoes a conventional Peierls transition at T_P = 215 K which is preceded by a sizeable regime of $2k_F$ BOW fluctuations [35]. These data show that the Peierls instability of the acceptor dithiolate stacks is achieved by a sizeable electron–phonon coupling as found for the donor stack in $(arene)_2$ PF_6 and AsF_6 salts. The presence of critical phonon modes coupled to electronic degrees of freedom at first order in molecular displacement should persist in S = 1/2 AF electron localized $[M(mnt)_2]$ chains. Via a magneto-elastic spin–phonon coupling, these modes should modulate the AF exchange coupling between dithiolate molecules. Such a modulation is the basic ingredient to obtain a stack dimerization allowing to pair spins $\frac{1}{2}$ into a SP ground state.

3.1. Spin-Peierls Structural Fluctuations

The key role of the lattice counterpart of the SP instability of the *M* = Ni, Pd and Pt dithiolate stacks is evidenced by the detection of a sizeable regime of 1D structural fluctuations appearing as diffuse lines of strong intensity located in b*/2 on X-ray diffuse patterns. Such diffuse lines have been observed in Pt ([9]—see also Figure 5a), Ni [23] and Pd [9] derivatives. The reduced critical wave vector of the fluctuations q_{SP} = b*/2 corresponds to an incipient instability towards a doubling (dimerization) of the dithiolate stack periodicity. This structural modulation should drive the pairing of neighboring S = 1/2 spins into magnetic singlets.

The above quoted diffuse lines have been detected below 30 K, 100 K and 100 K in the Pt, Ni and Pd salts, respectively. This onset temperature, given in Table 2, is taken as the SP mean-field temperature (T_{SP}^{MF}) of the dithiolate stacks. T_{SP}^{MF} is twice larger than the temperature at which Peierls fluctuations begin to manifest on Per stacks (i.e., T_ρ, in Table 2). This provides clear evidence that the SP instability on dithiolate stack starts before the Peierls instability on Per stack.

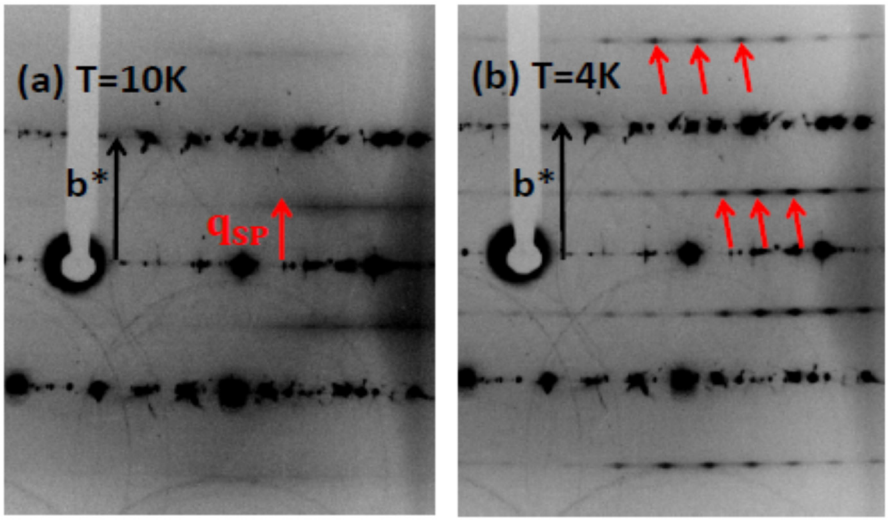

Figure 5. X-ray diffuse scattering patterns from α-$Per_2[Pt(mnt)_2]$ at: 10 K (**a**); and 4 K (**b**). In (**a**), 1D SP critical lattice fluctuations gives rise to intense diffuse lines located at half distance (i.e., at the reduced q_{SP} = b*/2 wave vector) between horizontal layers of main Bragg reflections. In (**b**), red arrows show that these lines have condensed into broad diffuse spots, corresponding to the establishment of a 3D SP SRO.

Table 2. Characteristics of α-$Per_2[M(mnt)_2]$ salts for M = Pt, Ni and Pd which exhibit both a Peierls and a spin-Peierls instability on the Per and dithiolate stacks respectively. The metal-insulator Peierls transition temperature (T_P) and the temperature of minimum of resistivity (T_ρ) are taken from electrical measurements of References [7,8]. The SP critical temperature and the nature of the short range (SRO) or long range (LRO) SP order detected below T_{SP} are indicated as well as the temperature range of observation of 1D SP fluctuations. "T_{SP}" is the temperature at which $\chi_{SP}^{-1}(q_{SP})$ and ξ_b^{-1} extrapolate to zero in the Ni and Pt derivatives. In the Pd derivative, T_{SP} is the true 3D SP transition at which $\chi_{SP}^{-1}(q_{SP})$ and ξ_b^{-1} vanish.

$Per_2[M(mnt)_2]$	T_P/T_{SP} (K)	b*/4 Peierls Modulation	b*/2 spin-Peierls Modulation	T_ρ (K)	1D SP Fluctuations
M = Pt	8.2/"7.5"	not observed	SRO in all directions	18	≤30 K
M = Ni	25/"25–45"	LRO	SRO in all directions	50	≤100 K
M = Pd	28/28	not observed	LRO	50–80	≤100 K

The SP structural fluctuations of Ni, Pd and Pt derivatives can be quantitatively analyzed from the thermal dependence of the intensity and profile (along the stack direction b) of the diffuse lines [9], namely from:

- The q_{SP} peak intensity $I(q_{SP})$, the $T/I(q_{SP})$ ratio gives a quantity proportional to the inverse SP structural susceptibility $\chi_{SP}^{-1}(q_{SP})$ (Figure 6).
- The half-width at half-maximum (corrected by the experimental resolution) directly gives the inverse coherence length of the SP fluctuation in stack direction ξ_b^{-1} (Figure 7).

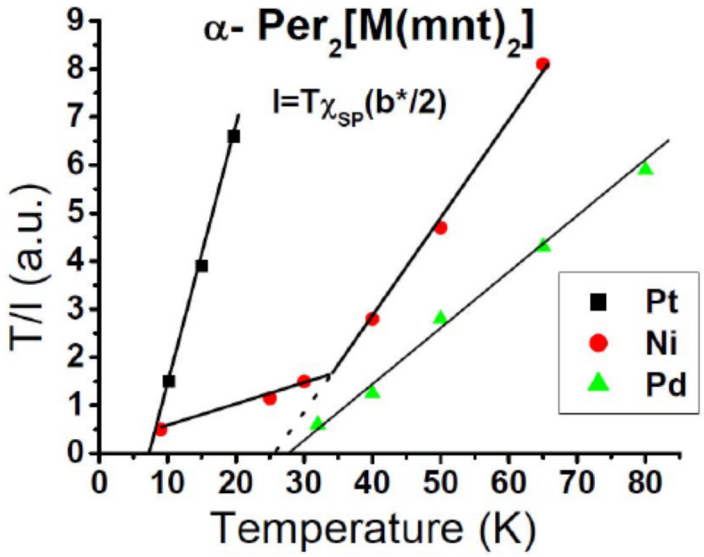

Figure 6. Temperature (T) dependence of the inverse spin-Peierls susceptibility $\chi_{SP}^{-1}(q_{SP})$ for the Ni, Pd and Pt derivatives. $\chi_{SP}^{-1}(q_{SP})$ follows basically a Curie–Weiss law (Equation (8). For the Ni salt, the dashed line extrapolates the thermal dependence of the high temperature data of $\chi_{SP}^{-1}(q_{SP})$ towards "T_{SP}".

$\chi_{SP}(q_{SP})$ exhibits a Curie–Weiss type divergence for the Pd and Pt salts as predicted for the high temperature fluctuations of the amplitude of the order parameter (i.e., regime of Gaussian fluctuations) [36]. The linear thermal dependence of the inverse susceptibility fitting the data, shown in Figure 6:

$$\chi_{SP}^{-1}(q_{SP}) \propto (T - T_{SP}) \tag{8}$$

allows defining T_{SP} at about 28 K and 7.5 K for the Pd and Pt salts. For the Ni salt, $\chi_{SP}^{-1}(q_{SP})$ changes slope upon cooling. Figure 6 shows that the high temperature data extrapolate to a "T_{SP}" of ~25 K.

The correlation length increases in an inverse square root law as predicted in the regime of Gaussian fluctuations of the amplitude of the order parameter [36]. The inverse correlation length, shown in Figure 7, is fitted by this square root thermal dependence:

$$\xi_b^{-1} \propto \sqrt{(T - T_{SP})} \tag{9}$$

The extrapolation at zero of Equation (9) leads to the same T_{SP} as does Equation (8) for the Pd and Pt salts.

For the Pd salt, $\chi_{SP}^{-1}(q_{SP})$ and ξ_b^{-1} vanish at T_{SP} = 28 K. Below T_{SP}, SP superstructure reflections are detected at the reciprocal wave vector component q_{SP} = b*/2 [9]. There is thus below T_{SP} = 28 K a long range SP order. The Pd salts thus exhibits all the structural characteristics of a well-defined 2nd order SP transition.

In the Pt salt, $\chi_{SP}^{-1}(q_{SP})$ and ξ_b^{-1} tend to vanish at about 7.5 K. However, the X-ray pattern taken at 4 K (Figure 5b) shows that only a SP SRO is achieved at low temperature. There is thus a pseudo-SP transition at "T_{SP} " ≈ 7.5 K as indicated in Table 2.

In the Ni salt, there is no vanishing of ξ_b^{-1} and $\chi_{SP}^{-1}(q_{SP})$.ξ_b^{-1} saturates below 50 K while the high temperature data extrapolate to zero around 45 K. $\chi_{SP}^{-1}(q_{SP})$ changes slope below 35 K while the high temperature data linearly extrapolate to zero around 45 K. These two "T_{SP}" extrapolation values are indicated in Table 2.

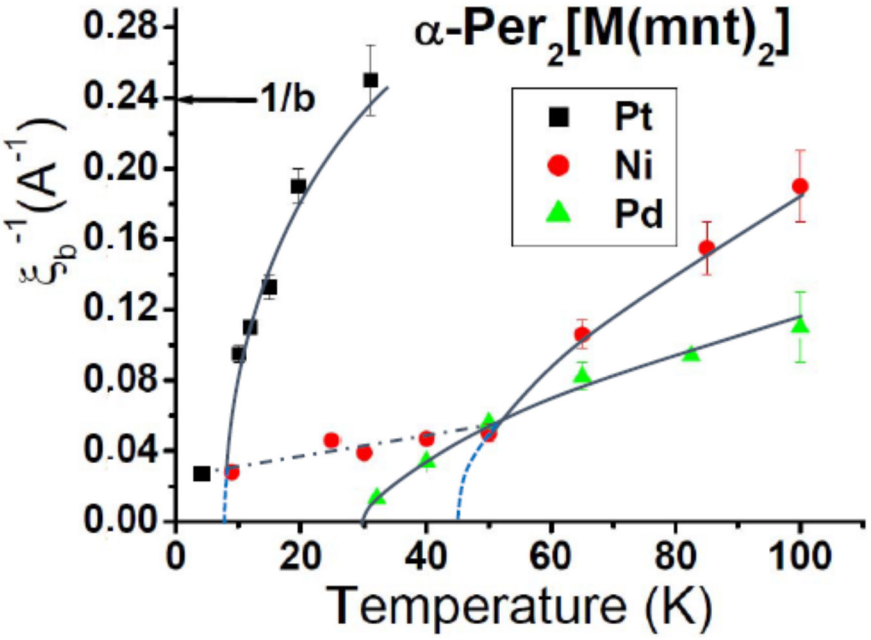

Figure 7. Temperature dependence of the inverse correlation length ξ_b^{-1} in stack direction for the Ni, Pd and Pt derivatives. For the Ni and Pt salts, the dashed lines extrapolate, using Equation (9), the thermal dependence of the high temperature data of ξ_b^{-1} towards "T_{SP}". The dotted dashed lines gives the low temperature saturation values of ξ_b^{-1} for the Ni and Pt salts.

3.2. Spin-Peierls and Peierls Orders

Table 2 gives the Peierls critical temperature (on Per stack) deduced from the metal to insulator transition detected by conductivity measurements [7,8]. Very weak $2k_F^D$ = b*/4 super-lattice reflections have been detected below T_P in the Ni salt [23]. They have an intensity comparable to those found below T_P in the Cu salt. No b*/4 super-lattice reflections have been detected in the Pd and Pt salts. They could be too weak to be detected.

T_{SP} and "T_{SP}" values reported in Table 2 are the temperature at which 1D SP fluctuations diverges or tends to diverge as discussed above. Sharp SP superstructure reflections, of longitudinal component q_{SP} = b*/2, are observed below T_{SP} = 28 K in the Pd salt [9].

"T_{SP}" is a pseudo SP transition temperature for the Ni salt since the low temperature saturation of $\chi_{SP}^{-1}(q_{SP})$ and ξ_b^{-1} reveals a short range dimerization order in all the directions [23]. At 9 K, the SP dimerization extends on 35 Å (i.e., 8b) in stack direction and a well-defined phasing between neighboring dimerization extend only on 14 Å in transverse directions. Fourteen Angstroms correspond to about the distance between first neighboring dithiolate stacks. Figure 2 shows that the transverse interaction between first neighbor dithiolate stacks should be mediated through a perylene stack. For this reason such a coupling should be weak, which explains why dimerization of only first neighbor dithiolate stacks are correlated in the SP ground state. Note that in the Ni derivative such a SP SRO cannot be due to disorder in the material because sharp b*/4 superstructure reflections are also observed. Since a similar SP SRO is observed in the Pt derivative (see below), the SRO has certainly an intrinsic origin.

A somewhat similar situation is observed in the Pt derivative. A specific heat anomaly indicates the occurrence of a thermodynamic phase transition around 8 K [37]. However, Table 2 indicates a T_P (8.2 K corresponding to the metal-insulator transition detected from transport measurements) distinct from "$T_{SP''}$ (7.5 K temperature at which 1D SP fluctuations tend to diverge and at which the EPR signal drop [38]). The finding of a T_{SP} distinct from T_P seems to be sustained by the extrapolation to 0 T of the magnetic phase diagram of the Pt salt [39].

The establishment of a low temperature spin-singlet ground state on [Pt(mnt)$_2$] chains is evident from EPR [38], ^{1}H NMR spectra and spin relaxation ($1/T_1$) rate [39,40] measurements. However, local magnetic measurements cannot probe the spatial extend of the SP order. Thus, a possible explanation of the decoupling between T_P and "T_{SP}" could rely on the fact that the SP dimerization order remains incomplete. The X-ray pattern shown in Figure 5b proves that there is not a long range SP dimerization at 4 K: the SP dimerization extends on 36 Å (i.e., 9b) in stack direction and 16 Å (i.e., the first neighbor dithiolate distance) in transverse direction. Note that these SP coherence lengths are comparable to those found in the Ni derivative. In addition, an incomplete SP pairing means that unpaired spins 1/2 should remain present. A minority of such spins has been recently identified by low temperature NMR measurements [41]. Note that the presence of low temperature unpaired spins agrees with the observation of a finite spin susceptibility in the SP ground state of the Pt salt [40,41].

The simultaneous presence of incomplete transverse and longitudinal SP orders and of unpaired spins $\frac{1}{2}$ can be rationalized using a previous interpretation of similar findings in doped $CuGeO_3$ SP systems [42]. In the SP ground state, the minimum of inter-chain coupling energy generally imposes an out of phase transverse phasing between dimerization on first neigbouring chains (this corresponds to a minimum of Coulomb coupling between dimerized charged chains). This minimum of energy implies that dimerization should be shifted by b between first neighboring chains. In presence of such a SP pattern, the staggered transverse order can be easily broken by keeping the dimerization of two first neighboring chains in phase. This linear defect, which consists of an absence of relative shift between dimerization located on two first neighbor chains, can be viewed as adding a local transverse phase shift of π in the SP pattern. This defect costs a maximum of inter-chain coupling energy. In that situation, the best way to limit this cost is to reduce the spatial extent of the linear defect by restoring the natural out of phase SP inter-chain order. This can be achieved by limiting the extent of the defect by ending the linear defect by two unpaired spins $\frac{1}{2}$. Each unpaired spin corresponds to a defect of dimerization which changes the phase of the intra-chain SP dimerization by $\pm\pi$. The creation of pairs of $\pm\pi$ dimerization defects thus limits the spatial extend of the longitudinal SP order (the average distance between the two dimerization defects being of the order of ξ_b). As each dimerization defect bears an unpaired spin $\frac{1}{2}$, the limitation of the SP order in chain direction implies a presence of S = 1/2 free spins. Such magnetic defects have been detected in the SP ground state of the Pt derivative. In our description, the limitation of the longitudinal order is caused by the break of the transverse order, but the reverse is also true. Generally, unpaired spins are created by any type of defect interrupting the spatial coherence of the longitudinal SP order.

3.3. Mechanism of the SP Instability in α-(Per)$_2$[M(mnt)$_2$]

Table 2 gives the temperature at which 1D SP fluctuations begin to be detected. This temperature is taken as the mean-field temperature of the SP transition $T_{SP}{}^{MF}$ [36]. One thus has $T_{SP}{}^{MF} \approx 30$ K for the Pt salts and 100 K for the Pd and Ni salts. $T_{SP}{}^{MF}$ is related to the mean field SP gap, Δ^{MF}, by the mean-field correspondence relationship, which can be expressed for the Heisenberg chain by [43]:

$$\Delta^{MF} \approx 2.47 k_B T_{SP}{}^{MF} \quad (10)$$

With the above quoted $T_{SP}{}^{MF}$ values, one gets $\Delta^{MF} \approx 75$ K for the Pt salts and $\Delta^{MF} \approx 250$ K for the Pd and Ni salts.

In this framework, the mechanism driving the SP transition depends on the relative value of the mean-field gap Δ^{MF} with respect to the q_{SP} critical phonon energy: $\hbar\Omega_C \approx 50$–100 K for TA-LA phonon frequencies in organics [44]. For the Heisenberg chain, the SP transition occurs in the classical (adiabatic) limit when $\hbar\Omega_C \leq \Delta^{MF}/2$ [45]. In the opposite limit of weak Δ^{MF}, $\hbar\Omega_C \geq \Delta^{MF}/2$, the SP transition occurs in the quantum (anti-adiabatic) limit. Note that if Δ^{MF} is too small, such that $\Delta^{MF} \leq 0.7\,\hbar\Omega_C$ [46], the zero point phonon quantum fluctuations kills the SP dimerization. In that case, the SP gap vanishes exponentially at a quantum critical point beyond which a spin liquid state

is stabilized. The 0 K phase diagram of the SP ground state of the AF Heisenberg chain is shown in Figure 8. This figure shows that the SP transition of Pd and Ni salts occurs in the adiabatic limit while the SP transition of the Pt salt occurs in the non-adiabatic limit.

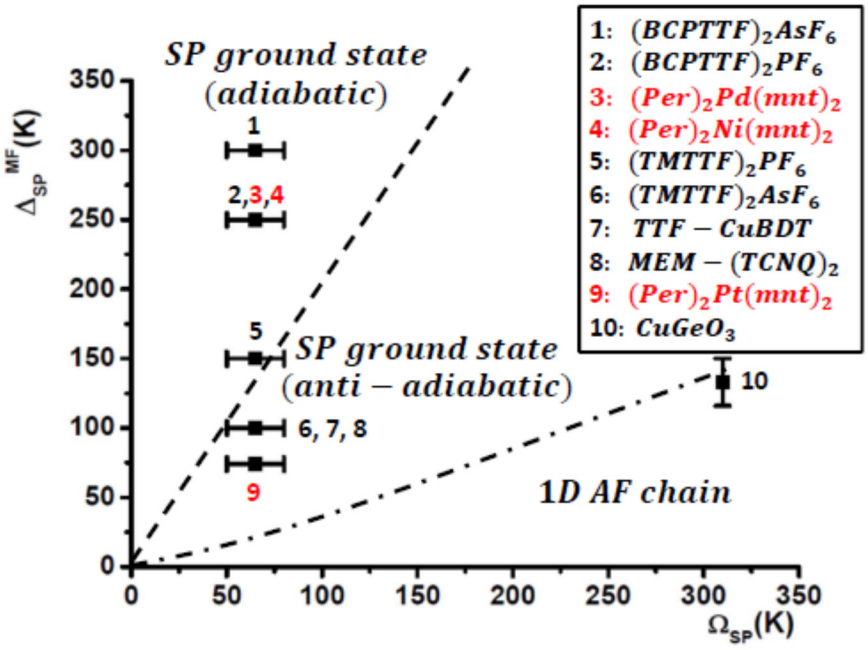

Figure 8. Nature of the SP ground state as a function of the mean-field gap, Δ_{MF} defined by Equation (7), and of the critical phonon frequency Ω_c for the SP Heisenberg chain (from [45]), together with the location of typical SP compounds (taken from Reference [3]). The α-$Per_2[M(mnt)_2]$ salts with M = Ni, Pd and Pt are indicated in red.

In the adiabatic limit, when the dynamics of SP structural fluctuations is slow compared to those of magnetic degrees of freedom, a local SP pairing, which develops below $T_{SP}{}^{MF}$ on ξ_b progressively forms a pseudo-gap in the density of states of magnetic excitations. This manifests by a depression in the thermal dependence of the spin susceptibility. In the opposite anti-adiabatic limit, the dynamics of SP structural fluctuations is so rapid that the spin susceptibility remains unaffected by the SP fluctuations until T_{SP}. A typical example of an adiabatic SP transition is the $(BCP\text{-}TTF)_2X$ series and of an anti-adiabatic SP transition is MEM-TCNQ [2,3,36,47] (BCP-TTF = benzocyclo-pentyl-tetrathiafulvalene; MEM = methyl-ethyl-morpholinium). Additional examples are given in Figure 8.

In order to analyze the influence of the SP structural instability on the spin degrees of freedom let us first consider the spin susceptibility, $\chi_S(T)$, of the Pd, Ni and Pt salts whose thermal dependence is shown in Figure 9a [8]. In a first approximation, the dithiolate sublattice can be described by a collection of isolated S = 1/2 AF chains. Then, each magnetic chain can be modeled by the simplest Heisenberg Hamiltonian:

$$H_{dith.} = J_1 \sum_j \boldsymbol{S}_j \boldsymbol{S}_{j+1} \tag{11}$$

where J_1 is the first neighbor exchange interaction. With such a Hamiltonian, the thermal dependence and the magnitude of the spin susceptibility $\chi_S(T)$ can be exactly calculated [48]. With this description Figure 9b gives at each temperature the effective first neighbor exchange interaction $J_{1\,eff}\,(T)$ taken from the absolute value of the spin susceptibility $\chi_S(T)$ for the Pd, Ni and Pt salts [49]. This figure shows in particular that:

- In the Pd salt, $J_{1\,eff}$ saturates at 260 K above 100 K.

- In the Pt salt, $J_{1\ eff}$ saturates at 35 K below 90 K.
- In the Ni salt, $J_{1\ eff}$ increases linearly between 300 and 100 K.

Figure 9b shows also deviations at these simple dependences. This means that Hamiltonian (Expression (9)) must be completed by additional contributions. Below we consider coupling of this Hamiltonian with SP structural fluctuations (as already considered in Reference [36]) and exchange coupling with conduction electron spins on Per stacks (as already considered in Reference [40]).

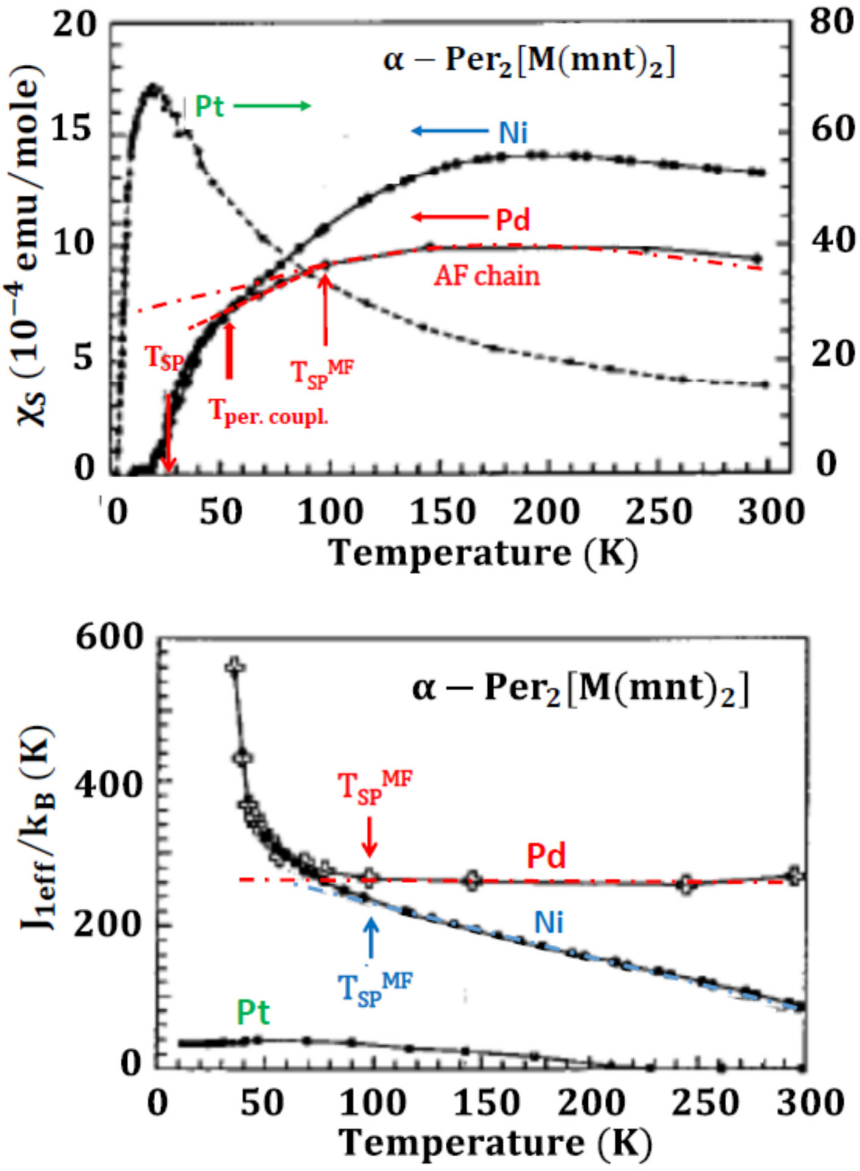

Figure 9. (**a**) Temperature dependence of the spin susceptibility, $\chi_S(T)$ of the Ni, Pd and Pt derivatives (**b**) Thermal dependence of the effective first neighbor AF exchange interaction $J_{1\ eff}\ (T)$ deduced from the amplitude of $\chi_S(T)$. In (**a**), $\chi_S(T)$ of the Pd derivative can be analyzed in the following way: (i) above $T_{SP}{}^{MF} \approx 100$ K $\chi_S(T)$ follows the thermal behavior of the 1D AF chain, (ii) between $T_{SP}{}^{MF}$ and $T_{per.\ coupl.} \approx 50$ K the slight drop of $\chi_S(T)$ is due to the development of a pseudo-gap caused by 1D SP fluctuations, and (iii) between $T_{per.\ coupl}$ and $T_{SP} \approx 28$ K the large drop of $\chi_S(T)$ is due to an enhancement of the singlet-triplet gap due to frustration of AF interactions. A 3D SP transition occurs at T_{SP}. In (**b**), note that the rapid increase of $J_{1\ eff}\ (T)$ below 100 K ($T_{SP}{}^{MF}$) occurs in the temperature range where SP fluctuations are present. (Part (a) is completed from data of reference [8] and part (b) is modified from reference [49]).

Let us start with the SP instability of the Pd salt which occurs in the adiabatic limit. For this salt relevant energies of its SP instability ($J_1 \approx 260$ K and $T_{SP}{}^{MF} \approx 100$ K) are comparable to those already reported in the (BCP-TTF)$_2X$ series ($J_1 \approx 270$ K, $T_{SP}{}^{MF} \approx 120$ K for $X = AsF_6$ and $J_1 \approx 330$ K, $T_{SP}{}^{MF} \approx 100$ K for $X = PF_6$ [47]). All these organic compounds have also similar critical phonon frequencies, Ω_C. Figure 9a shows that the spin susceptibility of the Pd salt behaves above 100 K as $\chi_S(T)$ of an S = 1/2 AF chain with $J_1 \approx 260$ K, which is also the case for (BCP-TTF)$_2X$. Below $T_{SP}{}^{MF} \approx 100$ K SP lattice fluctuations develop on the correlation length ξ_b (whose thermal dependence of its inverse is given in Figure 7) a local spin singlet S = 0 state. This local non-magnetic order induces below 100 K a pseudo-gap in the magnetic excitation spectrum which manifests (see Figure 9a) by a decrease of the spin susceptibility with respect to $\chi_S(T)$ of the uniform 1D AF chain when ξ_b increases. This feature corresponds to a net increase of $J_{1\ eff}$ below 100 K (see Figure 9b). This thermal behavior, which resembles to the one measured and calculated in (BCP-TTF)$_2$X salts, corresponds to the coupling of AF fluctuations to SP critical lattice fluctuations [36]. The drop of $\chi_S(T)$ is the same in the Pd derivative and in (BCP-TTF)$_2X$ between 100 K and 50 K. Below 50 K $\chi_S(T)$ of the Pd salt drops abruptly to nearly vanishes at $T_{SP} = 28$ K (Figure 9a), while $\chi_S(T)$ of (BCP-TTF)$_2X$ SP continues to decrease monotonously and remains finite at its SP transition [36,47]. Thus the vanishing of $\chi_S(T)$ below 50 K in the Pd derivative cannot be due to standard SP structural fluctuations which diverge continuously in temperature (see Figures 6 and 7) as those of (BCP-TTF)$_2X$ [36,47].

In order to account for the extra vanishing of $\chi_S(T)$ observed below 50 K in the Pd derivative, one has to consider some thermal dependent modification of magnetic exchange interactions on dithiolate stacks. Below we propose that such a modification arises from the AF exchange coupling between the localized spins $\boldsymbol{S}_j$ on dithiolate molecule "j" and the spin density $\boldsymbol{s}_l(x)$ on neighboring "l" metallic Per chain. Since the net decrease of $\chi_S(T)$ coincides with the development of a $2k_F$ density wave instability on the Per stack (which should grow below about $T_\rho \approx 50$–80 K—see Table 2) the new interaction appears to be driven by the onset of a collective response on the Per stacks below a quite well defined temperature, noted $T_{per.\ coupl}$ in Figure 9a, which is close to T_ρ. Below $T_{per.\ coupl}$, the $2k_F$ electron–hole instability on the Per stack, $\chi_{eh}\left(2k_F^D, T\right)$, submitted to an "external" AF field originating from the localized spins on dithiolate stacks responds by setting a $2k_F$ spin density wave (SDW) $\boldsymbol{s}_l(x)$, as schematically illustrated by Figure 10.

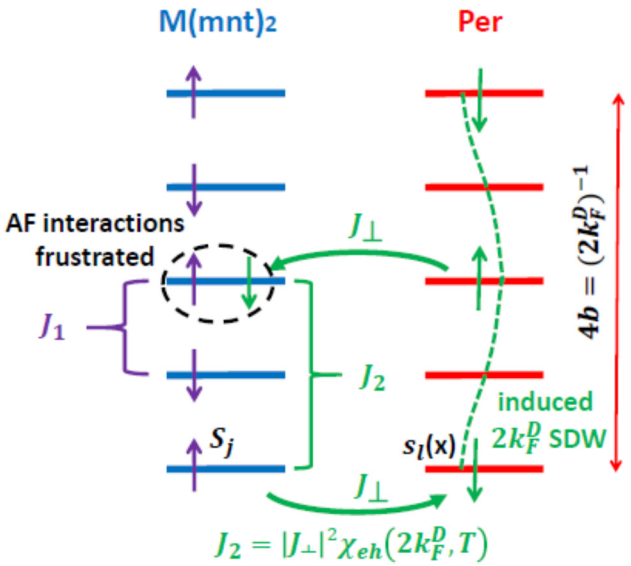

Figure 10. Schematic representation of competing AF S = 1/2 exchange couplings in α-Per$_2$[M(mnt)$_2$] derivatives for M = Ni, Pd and Pt. J_1 is the first neighbor direct exchange coupling on dithiolate stack. J_2 is the second neighbor indirect RKKY exchange coupling mediated by the induced $2k_F^D$ SDW on the Per stack.

Following the notations of Ref. [40], this additional interaction can be modeled by adding to the direct exchange Hamiltonian (Equation (11)) an inter-chain exchange coupling Hamiltonian involving the spins density $\boldsymbol{s}_l(x)$ on neighboring Per sacks:

$$H_{coupl.} = \sum_{l,\ per.} \int \left[H_l^{1D\ cond}(x) + J_\perp \sum_{j,\ dith.} \boldsymbol{S}_j \boldsymbol{s}_l(x) \right] dx \tag{12}$$

The first term of the right member of Equation (12) $H_l^{1D\ cond}(x)$ is the Hamiltonian of the 1D conduction electron gas located on the Per stack "l"; x being the stack direction. In the second right member of Equation (12) $J_\perp$ is the transverse exchange coupling between nearest dithiolate and per spins, respectively $\boldsymbol{S}_j$ and $\boldsymbol{s}_l(x)$. Note, as indicated in Figure 2, that there are three different types of $J_\perp$ interactions per Per (the strongest one should occur in the direction of maximum overlap of dithiolate and Per MOs). Experimental evidence for a sizeable transverse exchange coupling $J_\perp$, (or equivalently for a fast inter-chain spin exchange regime) is provided by the observation for Pd [50] and Pt [40] derivatives of a single EPR line at a g value intermediate between those of $[M(\mathrm{mnt})_2]$ and of Per molecules.

Due to the quasi-1D nature of its electron gas, the Per stack exhibits a divergent electron–hole response $\chi_{eh}\left(2k_F^D, T\right)$, which sizably grows below T_ρ for $2k_F^D = \mathrm{b}^*/4$. In this regime, a spin $\mathbf{S}^\circ$ located on a dithiolate molecule placed at the origin should polarize, through the AF exchange coupling $J_\perp$, the electronic spin density $\boldsymbol{s}_l\ (\boldsymbol{x})$ located on neighboring per stacks, as shown in Figure 10. This induces a SDW $s(x)$ on Per stacks whose thermal and spatial dependences are given by the 1D Fourier transform of $\chi_{eh}\left(2k_F^D, T\right)$ (assumed here to be that of a free electron gas):

$$s(x) \sim \chi_{eh}\left(2k_F^D, T\right) \frac{\cos(2k_F^D x)}{x} e^{-x/\xi_T} \tag{13}$$

In Expression (13), the SDW which oscillates with the period 4b is also damped by the thermal electronic length ξ_T issued from the thermal broadening of the FS. At a distance x = mb from the origin the oscillating spin density $s(x)$ exhibits, through $J_\perp$, a magnetic coupling with the spin $\mathrm{S^m}$ located on the near neighbor dithiolate molecule "m". Through the oscillating spin polarization of Per stack, this induces a spatially dependent effective exchange coupling between spins $\boldsymbol{S}^\circ$ and $\boldsymbol{S}^{\mathbf{m}}$ distant of mb on the same dithiolate stack. Such an indirect oscillating interaction is known in the literature as the Rudernann–Kittel–Kasuya–Yoshida (RKKY) interaction. It behaves basically in 1D as

$$J_{RKKY}^m\left(2k_F^D,\ T\right) \sim -|J_\perp| \chi_{eh}\left(2k_F^D, T\right) \frac{\cos(m\pi/2)}{m} e^{-mb/\xi_T} \tag{14}$$

Note that the spatial variation of the RKKY interaction is exactly given in 1D by $Si(2k_F x) - \pi/2$ where $Si(x)$ is the sine integral function (see Ref. [51]).

The mediated interaction (Expression (14)) provides in particular an indirect AF coupling between spins located on every second molecules (m = 2) on the dithiolate stack (note in Expression (14) that $J_{RKKY}^m\left(2k_F^D,\ T\right)$ does not depends on the sign of $J_\perp$). As shown in Figure 10 this indirect AF coupling competes with the intra-stack second neighbor effective ferromagnetic coupling due to the succession of two first-neighbor direct AF interaction J_1. Furthermore because of the 1D nature of the electron gas on Per stack $\chi_{eh}\left(2k_F^D, T\right)$ should diverge upon cooling (with a logarithmic thermal divergence for a 1D free electron gas). Thus the amplitude of the second neighbor AF interaction $J_{RKKY}^{m=2}\left(2k_F^D,\ T\right)$ is enhanced when T decreases and tends to overcome J_1.

1D magnetic chain with first, J_1, and second, J_2, neighbor frustrated AF interactions presents a very unusual phase diagram at 0 K (see for example [52]). When the ratio of exchange coupling $\alpha = J_2/J_1$ is smaller than $\alpha_c \approx 0.24$, the ground state is a gapless spin fluid state as for a simple Heisenberg chain, with a quasi-long range AF order. The nature of the ground state changes when $\alpha \geq \alpha_c$, through a quantum critical point located at α_c, into a spin gapped state with a long range dimer order. When the

ratio of exchange coupling α is larger than α_c a singlet-triplet gap opens in absence of any coupling with the phonon field. In the Pd salt, the rapid vanishing of the spin susceptibility observed below 50 K (Figure 9a) could be caused by the rapid growth of the ratio of exchange coupling α above α_c due to the thermal increase of $J^{m=2}_{RKKY}(2k^D_F,\ T)$ below T_ρ. However, as SP critical fluctuations continue to diverge upon cooling the total singlet-triplet gap should superimpose the effects of the SP lattice dimerization and of the frustration of AF coupling. Such combined effects have been considered in the literature [53,54].

The SP instability of the Ni salt also occurs in the adiabatic limit. There are however some differences between Ni and Pd salts. A noticeable difference is that $J_{1\ eff}(T)$ increases linearly when T decreases between 300 and 100 K (Figure 9b), while $J_{1\ eff}(T)$ is constant in the same temperature range for the Pd salt. It is thus possible that the increase of $J_{1\ eff}(T)$ results from an enhancement of the intra-molecular overlap between dithiolate MO due a continuous sliding of neighboring Ni(dmit)$_2$ molecules upon cooling. However in spite of this effect there is a net deviation at the linear increases of $J_{1\ eff}(T)$ below 100 K when SP critical fluctuations develops. This could be due, as for the Pd salt, to the growth of a pseudo-gap in the AF magnetic excitation spectrum. In addition, similarly to the Pd salt, $\chi_S(T)$ abruptly drops below 50 K and vanishes around 20 K (Figure 9a). Note however that if below 50 K $\chi_S(T)$ exhibits the same temperature dependence for the two salts, Figures 6 and 7 show that in the same temperature range SP critical structural fluctuations behave differently for the Ni and Pd derivatives. While SP fluctuations diverge at T_{SP} = 28 K in the Pd derivative, SP fluctuations reduce their divergence below ~ 50 K (for ξ_b) and ~35 K (for χ_{SP}) in the Ni derivative. Thus, the rapid decrease of $\chi_S(T)$ in the Ni derivative cannot be due to the critical growth of SP fluctuations. As $\chi_S(T)$ considerably decreases below $T_\rho \approx 50$ K when $\chi_{eh}(2k^D_F, T)$ sizably increases, the spin gap opening is more likely due to a frustration effect between second neighbor indirect $J^{m=2}_{RKKY}(2k^D_F,\ T)$ and first neighbor direct J_1 AF interactions on the Ni dithiolate stack as shown in Figure 10.

Figure 9a shows that the thermal dependence of $\chi_S(T)$ below ~40 K resembles that of a thermally activated excitation process. For an activated process through a gap Δ, the spin susceptibility of a classical assembly of spin $\frac{1}{2}$ behave as:

$$\chi_s(T) \propto \frac{1}{T} e^{-\Delta/T} \tag{15}$$

Data of Figure 9a give Δ ~130 K, which amount to about $J_1/2$. We thus propose that the gap which develops below 50 K is a singlet triplet gap mainly set by frustration effects between first and second neighbor AF interactions when $\alpha = J_1/J_2 \geq \alpha_c \approx 0.24$. Note that the opening of a gap $\Delta \sim J_1/2$ in absence of sizeable lattice dimerization requires a sizeable AF frustration ratio with α ~0.5 [54]. α = 0.5 corresponds to the so-called Majumdar–Ghosh point where the ground state of the AF chain, which corresponds to two possible dimerization patterns formed by a succession of disconnected singlet dimers, is twofold degenerate.

The magnetic properties of Pt salt have been already considered in Ref. [40] first suggesting the presence of mediated RKKY interactions through the Per stack. However, the physics of Pt salt differs on many aspects from the one exhibited by Pd and Ni salts. Firstly, the SP instability of the Pt salt occurs in the non-adiabatic limit. Thus, the development of critical structural SP fluctuations below 30 K ($T_{SP}{}^{MF}$) should not open a pseudo-gap in the spin excitations. Accordingly, the thermal dependence of $\chi_S(T)$ should not deviate appreciably between $T_{SP}{}^{MF}$ and T_{SP} from the extrapolated high temperature dependence of $\chi_S(T)$ (more precisely Figure 9b shows that $J_{1\ eff}$ does not change appreciably below 30 K). A similar behavior is shown by $\chi_S(T)$ in the non-adiabatic SP compound MEM-(TCNQ)$_2$ [2,3,47]. Secondly, SP fluctuations start below 30 K in the temperature range where the AF correlations are not developed (AF correlations develop when $\chi_S(T)$ begins to decrease below $\approx$ 20 K). The nature of the driving force of the SP instability in the Pt salt must be questioned because the SP instability should be triggered, in presence of AF correlations, by quantum fluctuations of the AF chain (i.e., in the temperature range below the maximum of $\chi_S(T)$).

All these features require a clarification of the various types of effective spin-spin interactions occurring on the Pt dithiolate stack. In particular and in addition to the first neighbor AF interaction J_1 (estimated at ~35 K from the fit of $\chi_S(T)$ shown in Figure 9b) additional AF interactions which competes with J_1 should be considered. Firstly, one expects to have below $T_\rho \approx 18$ K, when the electron–hole response of the Per stack develops a second neighbor mediated AF interaction $J_{RKKY}^{m=2}(2k_F^D,\ T)$ as for the Pd and Ni derivatives. Secondly in the non-adiabatic regime, the SP magneto-elastic coupling leads to a renormalization of J_1 and induces a second neighbor AF interaction J_2 [46]. For these two reasons the spin-spin Hamiltonian of the dithiolate stack should include first and second neighbor AF competing interactions which modify the thermal dependence of $\chi_S(T)$ when only J_1 is considered. This requires a more complete analysis of the thermal dependence of $\chi_S(T)$. However, as $\chi_S(T)$ does not decrease drastically on approaching T_{SP}, the frustration ratio $\alpha = J_1/J_2$ should be probably less than α_c, at the difference of Pd and Ni derivatives.

3.4. Nature of the Ground State

In the previous section, we have shown, especially for the Pd and Ni derivatives, that $Per_2[M(mnt)_2]$ salts exhibit magnetic properties on dithiolate stacks coupled to a $2k_F$ density wave instability of the conducting Per stacks. Such features place $Per_2[M(mnt)_2]$ among Kondo lattices where localized spins are coupled to itinerant spins of the conduction electron gas. Theory of 3D Kondo lattice based on Hamiltonians similar to the one given by (12) shows a competition between Kondo effect on each magnetic site and magnetic ordering arising from the RKKY interaction (see for example [55]). The Kondo effect, discovered in 1964 [56] by considering the interaction between a single magnetic impurity and conduction electrons, tends to stabilize a ground state characterized by the formation of a local singlet between the spin of conduction electrons and the spin of the impurity. In the Per-dithiolate series the 1D anisotropy of both the transfer integrals in the metallic subsystem and of the J_1 AF exchange coupling in the magnetic subsystem place $Per_2[M(mnt)_2]$ among the 1D Kondo lattices. Note also since, as shown in Figure 2, magnetic chains are spatially decoupled from the conducting chains that α-$Per_2[M(mnt)_2]$ belongs to the category of two-chain 1D Kondo lattices. In this respect α-$Per_2[M(mnt)_2]$ differs from standard one chain Kondo lattices where, because of the presence of several electron species, spin localized and conducting electrons are located on the same chain such as in metal-phthalo-cyanine-iodine Cu(pc)I [57] or $BaVS_3$ [58] There is an abundant literature on 1D Kondo lattices based on elaborated theoretical considerations [51,59]. However, experimental clear-cut evidence of 1D Kondo lattice effects are quite sparse in the literature. Following our present analysis $Per_2[M(mnt)_2]$ organic salts with M = Ni and Pd should be a good realization of 1D Kondo lattice physics.

In this framework, it has been previously proposed that spin dimerization observed in $Per_2[M(mnt)_2]$ salts could be explained using a 1D Kondo lattice model at quarter filling with some kind of RKKY interaction between localized moments [60]. However the realization of such a ground state is not obvious because it has been numerically shown that a frustrated spin-1/2 Heisenberg chain coupled to adiabatic phonons can exhibit a tetramerized phase for a large enough frustration ratio α and a large spin-lattice coupling [61]. These different theoretical finding show that the physics of $Per_2[M(mnt)_2]$ should be quite subtle because there are two competing periodicity in the system: $2k_F^D = b^*/4$ for the Peierls instability on the Per stack and $2k_F^{SP} = b^*/2$ for the SP instability on the dithiolate stack.

In presence of non-magnetic dithiolate stacks the Peierls transition stabilizes the $2k_F^D$ modulation as shown by experimental studies of M = Cu, Co and Fe compounds (Table 1). Complications arise in salts where with M = Ni, Pd and Pt the dithiolate stack is magnetic and where, with a sizeable magneto-elastic coupling, a SP instability develops at $2k_F^{SP}$, which is two times $2k_F^D$. In Ni, Pd and Pt salts there is no experimental evidence that both $2k_F^D$ and $2k_F^{SP}$ LRO are simultaneously stabilized. In the Ni derivative where frustration effects are more apparent there is below 25 K a $2k_F^D$ LRO and a $2k_F^{SP}$ SRO. It is thus possible that the $b^*/2$ SP divergence on the dithiolate stacks stops around

50–35 K when the sizably frustrated spin system (α ~0.5) becomes quite strongly coupled to the adiabatic phonon field. In that case, the system should prefer to be tetramerized as predicted in Ref. [61]. In $Per_2[Ni(mnt)_2]$ the $2k_F^D$ LRO was initially attributed to the Peierls modulation on the Per stack. However one cannot exclude that a component of this modulation should originate from a distortion of the $Ni(dmit)_2$ stacks. In the Pd derivative the situation is different because a $2k_F^{SP}$ LRO is detected without any evidence of a $2k_F^D$ Peierls LRO; a feature which remains to be explained. In the Pt derivative there is a short range SP order in all the directions (of spatial extend comparable to the one of the Ni derivative) but Figure 5b does not provide any evidence of a $2k_F^D$ = b*/4 Peierls modulation. However, such a Peierls modulation could be too weak to be detected because the Peierls gap is quite small (one expects from the relative magnitude of the Peierls gaps super-lattice reflections 3 times less intense in the Pt salt than those detected in the Ni salt). Note however that the existence of a CDW modulation in the Pt derivative is assessed by the observations of non-linear conductivity effect due to the sliding of CDWs under electric field [25].

A key parameter of control of the phase diagram of $Per_2[M(mnt)_2]$ relies on the presence of sizeable inter-stack coupling. A close inspection of the structure shown in Figure 2 shows that if there are many direct interactions between Per stacks [15] the interaction between dithiolate stacks should be mediated through Per stacks. Thus, if Per stacks are the source of RKKY mediated interactions between localized spins on dithiolate stacks, one expects induced $2k_F^D$ SDW fluctuations on Per stacks (Figure 10). Such SDW fluctuations should compete with $2k_F^D$ BOW/CDW fluctuations at the origin of the Peierls instability of the Per stack. Up to now, there is no evidence of such a magnetic instability on the Per stack. However, it is possible that the modulation of Per stacks below T_P should be a mixed $2k_F^D$ SDW-CDW as found in the magnetic ground state of $(TMTSF)_2PF_6$ [62,63]. This could arise in particular in the Pd derivative where standard $2k_F^D$ Peierls superstructure reflections have not been detected.

In addition, in order to establish the RKKY mediated interaction the setting of a $2k_F^D$ electron–hole response function on the Per stack is of fundamental importance because it tunes the magnitude of the indirect AF coupling interaction via its thermal divergence below T_ρ. As the Peierls instability starts on Per stacks below T_ρ, which is lower than $T_{SP}{}^{MF}$, one observes on Ni and Pd dithiolate stacks firstly a SP instability below $T_{SP}{}^{MF}$, then secondly below T_ρ a vanishing of the singlet-triplet gap due to the growth of frustrated 2nd neighbor AF interactions. If the $2k_F^D$ electron–hole instability develops at higher temperature, as found in the $(arene)_2$ PF_6/AsF_6 salts, AF frustration will be set before the start of the SP instability. Thus, with the opening of a high temperature singlet-triplet gap due to AF frustration, the driving force for the SP instability could not be activated. These features show that the magnetic properties of dithiolate stacks result from a fine tuning with the Peierls instability on Per stacks.

4. Conclusions

In this paper, we have extensively reviewed the structural properties of the α-$Per_2[M(mnt)_2]$ series of organic conductors. When the dithiolate stack is diamagnetic for M = Au or Cu or strongly dimerized for M = Co and Fe, the Per stack undergoes a $2k_F^D$ = b*/4 Peierls instability. However, the Peierls transition occurs at temperatures, T_P ~12–73 K, more than twice smaller than those T_P ~160–180 K found in other quarter-filled D_2X arene cation radical salts where D is either FA or substituted Per and X is a monovalent anion such as PF_6 and AsF_6. In the case of 1D S = 1/2 AF dithiolate stack for M = Ni, Pd and Pt, a SP instability develops at $2k_F^{SP}$ = b*/2. As this last wave vector is twice larger than $2k_F^D$, a very rich ground states is observed. The SP instability of Ni and Pd derivatives occurs in the classical limit with the formation of a pseudo-gap, in the AF magnetic excitations spectrum, driven by the growth of structural SP fluctuations below 100 K. Surprisingly, the spin susceptibility of these two salts drops below 50 K to finally vanish around 20 K. We attribute this unexpected behavior to the development of a singlet-triplet gap caused by frustration of S = 1/2 AF interactions on dithiolate stacks. Frustration is attributed to the presence of a second neighbor indirect RKKY S = 1/2 AF interaction mediated by a fine tuning with the $2k_F^D$ electron–hole instability

of the Per stack. This subtle coupling between magnetic and conducting chains shows that the family of α-$Per_2[M(mnt)_2]$ compounds provides for their Ni and Pd derivatives a remarkable realization of 1D Kondo lattices. A somewhat different magnetic behavior, with no clear-cut manifestation of the 1D Kondo lattice effects, is observed in the Pt derivative whose SP instability occurs in the quantum limit.

Acknowledgments: Earlier structural studies reported in this review have been performed by Vasco da Gama, Rui Henriques, Vita Ilakovac and Sylvain Ravy. One of us (JPP) recognizes very fruitful discussions with Claude Bourbonnais.

Conflicts of Interest: The authors declare no conflict of interest.

References

1. Comès, R.; Lambert, M.; Launois, H.; Zeller, H.R. Evidence for a Peierls Distortion or a Kohn Anomaly in One-Dimensional Conductors of the Type $K_2Pt(CN)_4Br_{0.30}.xH_2O$. *Phys. Rev. B* **1973**, *8*, 571–575. [CrossRef]
2. Pouget, J.-P. Bond and charge ordering in low-dimensional organic conductors. *Phys. B* **2012**, *407*, 1762–1770. [CrossRef]
3. Pouget, J.-P. The Peierls instability and charge density wave in one-dimensional electronic conductors. *C. R. Phys.* **2016**, *17*, 332–356. [CrossRef]
4. Schlenker, C.; Dumas, J.; Greenblatt, M.; van Smaalen, S. (Eds.) Physics and Chemistry of Low-Dimensional Inorganic Conductors. In *Nato ASI Ser. B Phys*; Plenum: New York, NY, USA, 1996; Volume 354.
5. Pouget, J.-P. Interplay between electronic and structural degrees of freedom in quarter-filled low dimensional conductors. *Phys. B* **2015**, *460*, 45–52. [CrossRef]
6. Akamatsu, A.; Inokuchi, H.; Matsunaga, Y. Electrical Conductivity of the Perylene-Bromine Complex. *Nature* **1954**, *173*, 168–169. [CrossRef]
7. Almeida, M.; Henriques, R.T. Perylene Based Conductors. Chapter 2. In *Handbook of Organic Conductive Molecules and Polymers Volume 1 "Charge Transfer Salts, Fullerenes and Photoconductors"*; Nalva, H.S., Ed.; John Wiley & Sons Ltd.: Chichester, UK, 1997; pp. 87–149.
8. Gama, V.; Henriques, R.T.; Bonfait, G.; Almeida, M.; Ravy, S.; Pouget, J.P.; Alcacer, L. The interplay between conduction electrons and chains of localized spins in the molecular metals $(Per)_2M(mnt)_2$, *M* = Au, Pt, Pd, Ni, Cu, Co and Fe. *Mol. Cryst. Liq. Cryst.* **1993**, *234*, 171–178. [CrossRef]
9. Henriques, R.T.; Alcacer, L.; Pouget, J.P.; Jérome, D. Electrical conductivity and x-ray diffuse scattering study of the family of organic conductors $(perylene)_2M(mnt)_2$, (*M* = Pt, Pd, Au). *J. Phys. C Solid State Phys.* **1984**, *17*, 5197–5208. [CrossRef]
10. Monchi, K.; Poirier, M.; Bourbonnais, C.; Matos, M.J.; Henriques, R.T. The Peierls transition in $Per_2[Au_xPt_{1-x}(mnt)_2]$: Pair-breaking field effects. *Synth. Met.* **1999**, *103*, 2228–2231. [CrossRef]
11. Almeida, M.; Gama, V.; Santos, I.C.; Graf, D.; Brooks, J.S. Counterion dimerisation effects in the two-chain compound $(Per)_2[Co(mnt)_2]$: Structure and anomalous pressure dependence of the electrical transport properties. *CrystEngComm* **2009**, *11*, 1103–1108. [CrossRef]
12. Santos, I.C.; Gama, V.; Silva, R.A.L.; Almeda, M. to be submitted (2017).
13. Ilakovac, V.; Ravy, S.; Moradpour, A.; Firlej, L.; Bernier, P. Disorder and electronic properties of substituted perylene radical-cation salts. *Phys. Rev. B* **1995**, *52*, 4108–4122. [CrossRef]
14. Emery, V.J.; Bruinsma, R.; Barisic, S. Electron-Electron Umklapp Scattering in Organic Superconductors. *Phys. Rev. Lett.* **1982**, *48*, 1039–1043. [CrossRef]
15. Canadell, E.; Almeida, M.; Brook, J. Electronic band structure of α-$(Per)_2M(mnt)_2$ compounds. *Eur. Phys. J. B* **2004**, *42*, R453. [CrossRef]
16. Ilakovac, V.; Ravy, S.; Pouget, J.P.; Riess, W.; Brűtting, W.; Schwoerer, M. CDW instability in the 2/1 organic conductor $(FA)_2PF_6$. *J. Phys. IV Fr.* **1993**, *3*, C2-137–C2-140. [CrossRef]
17. Peven, P.; Jérome, D.; Ravy, S.; Albouy, P.A.; Batail, P. Physical properties of the quasi-one dimensional substituted perylene cation radical salt. *Synth. Met.* **1988**, *17*, B405–B410. [CrossRef]
18. Ilakovac-Casses, V. Etude de l'influence du désordre sur les instabilités et les propriétés physiques des conducteurs et supraconducteurs organiques. Thesis, Université Paris-Sud, Orsay, France, 1994.
19. Reiss, W.; Schmid, W.; Gmeiner, J.; Schwoerer, M. Observation of charge density wave transport phenomena in the organic conductor $(FA)_2PF_6$. *Synth. Met.* **1991**, *41–43*, 2261–2267.

20. Reiss, W.; Brűtting, W.; Schwoerer, M. Charge transport in the quasi-one-dimensional organic charge density wave conductor (Fluorenthene)$_2$PF$_6$. *Synth. Met.* **1993**, *55–57*, 2664–2669. [CrossRef]
21. Lopes, E.B.; Matos, M.J.; Henriques, R.T.; Almeida, M.; Dumas, J. Charge density wave non-linear transport in the molecular conductor (Perylene)$_2$Au(mnt)$_2$ (mnt = maleonitriledithiolate). *Europhys. Lett.* **1994**, *27*, 241–246. [CrossRef]
22. Ilakovac, V.; Ravy, S.; Pouget, J.P.; Lenoir, C.; Boubekeur, K.; Batail, P.; Dolanski Babic, S.; Biskup, N.; Korin-Hamzic, B.; Tomic, S.; Bourbonnais, C. Enhanced charge localization in the organic alloys [(TMTSF)$_{1-x}$ (TMTTF)$_x$]$_2$ReO$_4$. *Phys. Rev. B* **1994**, *50*, 7136–7139. [CrossRef]
23. Gama, V.; Henriques, R.T.; Almeida, M.; Pouget, J.-P. Diffuse X-ray scattering evidence for Peierls and "spin-Peierls" like transitions in the organic conductors (Perylene)$_2M$(mnt)$_2$ [M = Cu, Ni, Co and Fe]. *Synth. Met.* **1993**, *55–57*, 1677–1682. [CrossRef]
24. Gama, V.; Henriques, R.T.; Almeida, M.; Bourbonnais, C.; Pouget, J.-P.; Jérome, D.; Auban-Senzier, P.; Gotschy, B. Structual and magnetic investigations of the Peierls transition of α-(Per)$_2M$(mnt)$_2$ with M = Fe and Co. *J. Phys. I Fr.* **1993**, *3*, 1235–1244. [CrossRef]
25. Lopes, E.B.; Matos, M.J.; Henriques, R.T.; Almeida, M.; Dumas, J. Charge Density Wave Dynamics in Quasi-One Dimensional Molecular Conductors: a Comparative Study of (Per)$_2M$(mnt)$_2$ with M = Au, Pt. *J. Phys. I Fr.* **1996**, *6*, 2141–2149. [CrossRef]
26. Bonfait, G.; Matos, M.J.; Henriques, R.T.; Almeida, M. The Peierls transition under high magnetic field. *Physics B* **1995**, *211*, 297–299. [CrossRef]
27. Graf, D.; Brooks, J.S.; Choi, E.S.; Uji, S.; Dias, J.C.; Almeida, M.; Matos, M. Suppression of a charge-density-wave ground state in high magnetic fields: Spin and orbital mechanisms. *Phys. Rev. B* **2004**, *69*, 125113. [CrossRef]
28. Brooks, J.S.; Graf, D.; Choi, E.S.; Almeida, M.; Dias, J.C.; Henriques, R.T.; Matos, M. Magnetic field dependence of CDW phases in Per$_2M$(mnt)2 (M = Au, Pt). *J. Low Temp. Phys.* **2006**, *142*, 787–803. [CrossRef]
29. Brooks, J.S.; Graf, D.; Choi, E.S.; Almeida, M.; Dias, J.C.; Henriques, R.T.; Matos, M. Magnetic field dependent behavior of the CDW ground state in Per$_2M$(mnt)2 (M = Au, Pt). *Curr. Appl. Phys.* **2006**, *6*, 913–918. [CrossRef]
30. Hasegawa, Y.; Fukuyama, H. A theory of phase transition in quasi-one-dimensional electrons. *J. Phys. Soc. Jpn.* **1986**, *55*, 3978–3990. [CrossRef]
31. Graf, D.; Brooks, J.S.; Almeida, M.; Dias, J.C.; Uji, S.; Terashima and Kimata, M. Evolution of superconductivity from a charge-density-wave ground state in pressurized (Per)$_2$ [Au(mnt)$_2$]. *Europhys. Lett.* **2009**, *85*, 27009. [CrossRef]
32. Shirane, G.; Shapiro, S.M.; Comès, R.; Garito, A.F.; Heeger, A.J. Phonon dispersion and Kohn anomaly in tetratiafulvalene-tetracyanoquinodimethane (TTF-TCNQ). *Phys. Rev. B* **1976**, *14*, 2325–2334. [CrossRef]
33. Caron, L.G.; Bourbonnais, C. Two-cutoff renormalization and quantum versus classical aspects for the one-dimensional electron-phonon system. *Phys. Rev. B* **1984**, *29*, 4230–4241. [CrossRef]
34. Goze, F.; Audouard, A.; Brossard, L.; Laukhin, V.N.; Ulmet, J.P.; Doublet, M.L.; Canadell, E.; Pouget, J.P.; Zavodnik, V.E.; Shibaeva, R.P.; et al. Magnetoresistance in pulsed fields, band structure calculations and charge density wave instability in (TSeT)$_2$Cl. *Synth. Met.* **1995**, *70*, 1279–1280. [CrossRef]
35. Ahmad, M.M.; Turner, D.J.; Underhill, A.E.; Jacobsen, C.S.; Mortensen, K.; Carneiro, K. Physical properties and the Peierls instability of Li$_{0.82}$[Pt(S$_2$C$_2$(CN)$_2$)$_2$]. 2H$_2$O. *Phys. Rev. B* **1984**, *29*, 4796–4799. [CrossRef]
36. Dumoulin, B.; Bourbonnais, C.; Ravy, S.; Pouget, J.P.; Coulon, C. Fluctuation effects in low-dimensional spin-Peierls systems: Theory and experiment. *Phys. Rev. Lett.* **1996**, *76*, 1360–1363. [CrossRef] [PubMed]
37. Bonfait, G.; Matos, M.J.; Henriques, R.T.; Almeida, M. Spin-Peierls instability in Per$_2$[M(mnt)$_2$] compounds probed by specific heat. *J. Phys. IV Colloq.* **1993**, *3*, 251–254. [CrossRef]
38. Henriques, R.T.; Alcacer, L.; Almeida, M.; Tomic, S. Transport and magnetic properties on the family of perylene-dithiolate conductors. *Mol. Cryst. Liq. Cryst.* **1985**, *120*, 237–241. [CrossRef]
39. Green, E.L.; Brooks, J.S.; Kuhns, P.L.; Reyes, A.P.; Lumata, L.L.; Almeida, M.; Matos, M.J.; Henriques, R.T.; Wright, J.A.; Brown, S.E. Interaction of magnetic field-dependent Peierls and spin-Peierls ground states in (Per)$_2$[Pt(mnt)$_2$]. *Phys. Rev. B* **2011**, *84*, 121101(R). [CrossRef]
40. Bourbonnais, C.; Henriques, R.T.; Wzietek, P.; Kongeter, D.; Voiron, J.; Jerome, D. Nuclear and electronic resonance approaches to magnetic and lattice fluctuations in the two-chain family of organic compounds (perylene)$_2$ [M(S$_2$C$_2$(CN)$_2$)$_2$] (M = Pt, Au). *Phys. Rev. B* **1991**, *44*, 641–651. [CrossRef]

41. Green, E.L.; Lumata, L.L.; Brooks, J.S.; Kuhns, P.; Reyes, A.; Brown, S.E.; Almeida, M. ^{1}H and ^{195}Pt NMR Study of the Parallel Two-Chain Compound $Per_2[Pt(mnt)_2]$. *Crystals* **2012**, *2*, 1116–1135. [CrossRef]
42. Pouget, J.-P.; Ravy, S.; Schoeffel, J.P.; Dhalenne, G.; Revcolevschi, A. Spin-Peierls lattice fluctuations and disorders in $CuGeO_3$ and its solid solutions. *Eur. Phys. J. B* **2004**, *38*, 581–598. [CrossRef]
43. Orignac, E.; Chitra, R. Mean-field theory of the spin-Peierls transition. *Phys. Rev. B* **2004**, *70*, 214436. [CrossRef]
44. Pouget, J.P. Microscopic interactions in CuGeO3 and organic Spin-Peierls systems deduced from their pretransitional lattice fluctuations. *Eur. Phys. J. B* **2001**, *20*, 321–333, and 2001, *24*, 415. [CrossRef]
45. Citro, R.; Orignac, E.; Giamarchi, T. Adiabatic-antiadiabatic crossover in a spin-Peierls chain. *Phys. Rev. B* **2005**, *72*, 024434. [CrossRef]
46. Weiβe, A.; Hager, G.; Bishop, A.R.; Fehske, H. Phase diagram of the spin-Peierls chain with local coupling: Density-matrix renormalization-group calculations and unitary transformations. *Phys. Rev. B* **2006**, *74*, 214426.
47. Liu, Q.; Ravy, S.; Pouget, J.P.; Coulon, C.; Bourbonnais, C. Structural fluctuations and spin-Peierls transitions revisited. *Synth. Met.* **1993**, *55–57*, 1840–1845. [CrossRef]
48. Eggert, S.; Affleck, I.; Takahashi, M. Susceptibility of the Spin 1/2 Heisenberg Antiferromagnetic Chain. *Phys. Rev. Lett.* **1994**, *73*, 332–335. [CrossRef] [PubMed]
49. Gama, V. O Papel das Cadeias Conductoras e das Cadeias Magnéticas nos Compostos da Familia $Per_x[M(mnt)2]$ (x = 2, M = Cu, Ni, Co e Fe; x = 1, M = Co). Thesis, Universidade Técnica de Lisboa, Lisbon, Portugal, 1993.
50. Alcacer, L.; Maki, A.H. Magnetic Properties of Some Electrically Conducting Perylene-Metal Dithiolate Complexes. *J. Phys. Chem.* **1976**, *80*, 1912–1916. [CrossRef]
51. Gulácsi, M. The one-dimensional Kondo lattice model at partial band filling. *Adv. Phys.* **2004**, *53*, 769–937. [CrossRef]
52. Nomura, K.; Okamoto, K. Critical properties of S = 1/2 antiferromagnetic XXZ chain with next-nearest-neighbour-interactions. *J. Phys. A Math. Gen.* **1994**, *27*, 5773–5788. [CrossRef]
53. Augier, D.; Poilblanc, D. Dynamical properties of low-dimensional $CuGeO_3$ and NaV_2O_5 spin-Peierls systems. *Eur. Phys. J. B* **1998**, *1*, 19–28. [CrossRef]
54. Watanabe, S.; Yokoyama, H. Transition from Haldane Phase to Spin Liquid and Incommensurate Correlation in Spin-1/2 Heisenberg chains. *J. Phys. Soc. Jpn.* **1999**, *68*, 2073–2097. [CrossRef]
55. Coqblin, B.; Nüñez-Reigeiro, M.D.; Theumann, A.; Iglesias, J.R.; Magalhães, S.G. Theory of the Kondo lattice: competition between Kondo effect and magnetic order. *Philos. Mag.* **2006**, *86*, 2567–2580. [CrossRef]
56. Kondo, J. Resistance Minimum in Dilute Magnetic Alloys. *Prog. Theor. Phys.* **1964**, *32*, 37–49. [CrossRef]
57. Quirion, G.; Poirier, M.; Liou, K.K.; Ogawa, M.; Hoffman, B.M. Possibility of a one-dimensional Kondo system in the alloys of Cu_xNi_{1-x} (Phtalocyaninato)I. *J. Phys. (Paris) Colloq.* **1988**, *49*, C8-1475–C8-1476. [CrossRef]
58. Foury-Leylekian, P.; Leininger, P.; Ilakovac, V.; Joly, Y.; Bernu, S.; Fagot, S.; Pouget, J.P. Ground state of the quasi-1D correlated correlated electronic system $BaVS_3$. *Physics B* **2012**, *407*, 1692–1695. [CrossRef]
59. Tsunetsugu, H.; Sigrist, M.; Ueda, K. The ground-state phase diagram of the one-dimensional Kondo lattice model. *Rev. Mod. Phys.* **1997**, *69*, 809–863. [CrossRef]
60. Xavier, J.C.; Pereira, R.G.; Miranda, E.; Affleck, I. Dimerization Induced by the RKKY Interaction. *Phys. Rev. Lett.* **2003**, *90*, 247204. [CrossRef] [PubMed]
61. Becca, F.; Mila, F.; Poilblanc, D. Teramerization of a frustrated spin-1/2 chain. *Phys. Rev. Lett.* **2003**, *91*, 067202. [CrossRef] [PubMed]
62. Pouget, J.P.; Ravy, S. Structural Aspects of the Bechgaard Salts and Related Compounds. *J. Phys. I Fr.* **1996**, *6*, 1501–1525. [CrossRef]
63. Pouget, J.P.; Ravy, S. X-ray evidence of charge density wave modulations in the magnetic phases of $(TMTSF)_2PF_6$ and $(TMTTF)_2Br$. *Synth. Met.* **1997**, *85*, 1523–1528. [CrossRef]